IEEE Access
Multidisciplinary | Rapid Review | Open Access Journal

Received May 4, 2021, accepted May 14, 2021, date of publication May 19, 2021, date of current version May 26, 2021.

Digital Object Identifier 10.1109/ACCESS.2021.3081676

Inertia Response Coordination Strategy of Wind Generators and Hybrid Energy Storage and Operation Cost-Based Multi-Objective Optimizing of Frequency Control Parameters

TOHID RAHIMI[1], (Member, IEEE), LEI DING[1], (Senior Member, IEEE), MOSTAFA KHESHTI[1], (Member, IEEE), RASOUL FARAJI[1], (Member, IEEE), JOSEP M. GUERRERO[2], (Fellow, IEEE), AND GIBRAN DAVID AGUNDIS TINAJERO[2], (Member, IEEE)

[1]Key Laboratory of Power System Intelligent Dispatch and Control, School of Electrical Engineering, Ministry of Education, Shandong University, Jinan 250061, China

[2]Department of Energy Technology, Aalborg University, 9220 Aalborg, Denmark

Corresponding author: Tohid Rahimi (rahimitohid@yahoo.com)

This work was supported in part by the China Postdoctoral Science Foundation under Grant 2019M662357 and Grant 2019M662356, in part by the National Natural Science Foundation of China under Grant 52050410445, in part by the Innovation Project of Shandong Province under Grant 201901002, and in part by the Project of Shandong Province New and Old Kinetic Energy Conversion. The work of Josep M. Guerrero and Gibran David Agundis Tinajero was supported by the VILLUM FONDEN, Center for Research on Microgrids (CROM), under the VILLUM Investigator Grant 25920.

ABSTRACT Due to the high penetration of renewable energy resources in microgrids (MGs), the grid inertia becomes low which leads to the grid to be vulnerable to large disturbances. The energy storage devices can play an important role to enhance the inertia of MGs. However, due to the high investment cost of storages or their *dp/dt* limitation, the installed energy storages cannot cover the challenge of high *df/dt*. A prominent solution to solve the problem is to use the inertia response of the wind generators. However, relatively high second frequency nadir is the main drawback of using the inertia response of the wind generators which may impose an extensive disturbance to MGs. Accordingly, a coordinated operation strategy for MGs between wind generator and hybrid energy storage (HES) system is proposed in this paper. In addition, to improve the inertia response of the MG; providing high-quality communication infrastructures with low delay and increasing the Ultracapacitor capacity have been paid attention. In this paper, the costs of the installed Ultracapacitor and quality of communication services are defined as the operation cost. Guaranteeing enough frequency damping for the MG with low operation cost are two conflict objectives. Therefore, a multi-objective optimization method is used to set the controllers' values and reduce the operation cost. The results confirmed that the effectiveness of the proposed strategy to control hybrid power storage in coordination with the wind generator and the frequency recovery process is improved. Also, employing the optimum values guaranteed the frequency damping effectively with low operation cost. The Integral Absolute Error (IAE) value and operation cost are reduced by 13.6% and 32%, respectively. Also, the simulation results show that the maximum MG frequency deviation and maximum *df/dt* is well compatible with different standards in the presence of load perturbations and different wind speeds.

INDEX TERMS Microgrid (MG), frequency control, wind generator, hybrid energy storage (HES), ultra-capacitor, inertia response, multi-objective optimization.

I. INTRODUCTION

Nowadays, the design trend of conventional power systems is toward to use small power systems which are called MG. The use of MGs has been accelerated due to their many benefits such as reliability, resilience, cost savings and increasing grid ability to operate under fault conditions. MGs have the capability to integrate the Distributed Energy Resources (DER), which includes Energy Storage Systems (ESS), controllable loads and communication platforms [1], [2]. MGs combine

The associate editor coordinating the review of this manuscript and approving it for publication was S. Ali Arefifar.

clean and cost-effective renewable energy resources with reliable generator sets which can meet the requirements of the future power industry [3]. These grids have the capability to operate in long-term or short-term independently from the upstream grid because the variety of distributed generations and energy storage resources are available in these grids. Thus, they are free from irreparable damage caused by upstream network faults [4]. The ability to store energy, buy-sell energy at different times increase the economic justification of MGs. Due to their high reliability, they are suitable for critical applications such as hospitals and main grids [5].

In today's world, the deleterious effects of greenhouse gas emission from fossil fuel power plants have attracted a lot of attention, but significant reduction of using these pollutants from heating and transportation systems have not yet possible according to present and future conditions. Modern societies are moving toward the use of renewable energy sources [6]. These sources are connected to the grid with power electronic based interfaces [7]–[9]; however, the high penetration of renewable energy sources may impose challenges to critical frequency stability. Generally, renewable energy resources have little or no inertial response. Therefore, replacing conventional resources with renewable energy resources reduces the overall inertia of the system. Renewable energy sources penetration which commonly cannot participate in frequency control has been increased. This issue is targeted for higher penetration in power grids in the future. Thus, the number of other energy units that provide controllable power for primary and secondary control, decreases and as a result, the frequency deviation would increase [10]. To overcome the challenges of frequency instability, renewable energy resources must be developed so that they can participate in frequency regulation and increase system stability [11]. In off-grid MGs, DERs are used to regulate power and load perturbations by injecting or absorbing power result in adjusting the frequency of the MG. Adjusting the output power of controllable power resources can improve the damping frequency oscillations [12], [13]. Nevertheless, due to inherent delays in power supplies and limitations in power generation or consumption, power resources cannot respond to disturbances immediately. Thus, frequency fluctuations in the MGs can occur. To minimize the negative impact of the high penetration of renewable energy sources, different frequency control methods and inertia response of energy sources techniques for renewable energy sources with [14]–[16] and without [17], [18] employing energy storage systems are considered in the previous researches. So that renewable sources such as wind turbines and photovoltaic units can participate in frequency regulation [19].

Nowadays, realizing high penetrated wind base MGs is not far from expectation. However, low inertia of the MGs, sudden frequency drop in case of significant power disturbances, result in cascade failures are challenges of the MGs using renewable energy sources. Using the capability of the wind turbines contribution in inertia response and primary frequency control is one of the solutions. To overcome high frequency deviation in wind farm based MGs, some papers use deloading operation mode for the wind turbines to provide fast virtual inertia and primary frequency support for the MGs [20]–[28]. In [23], [24], [26], and [27], the controller gains are tuned with respect to the wind speed. The wind speed estimation methods are not precise methods and impose uncertainties to the controllers. However, by keeping the operation point of the wind turbines in deloding points [20]–[28], large derivable power of the wind turbines would be lost which may not cost-effective solutions for wind farm owners.

To cover the delaoding operation techniques, using the kinetic energy of wind generators in inertia response is another approach [29]–[36]. References [31]–[33] utilized an improved power-rotor speed trajectory curve with using *df/dt* term is proposed to provide frequency support and positive damping during frequency events. In these methods, a point in which the mechanical and electrical power equal is required. Thus, these methods implementation, due to wind speed variations and other mechanical and electrical uncertainties, in real systems is difficult. Implementation of stepwise inertia control is utilized in [34], [35] to prevent high rate of frequency change. However, relatively high second frequency nadir is the main drawback of this method. Due to low inertia of MGs, the second nadir may impose very large disturbance to MGs. It should mention that the majority of works that discussed in [29]–[36] did not consider the limitation on the rate of change of inertia power of wind.

To use saved kinetic energy of wind turbines with less challenges, coordination operation of the wind turbines and energy storages is utilized in the literature [37]–[41], which suffer some disadvantages. But [37], [39] do not give any solution to charge the ultra-capacitor to be ready to participate in case of successive frequency drop perturbations. As regards delivery of absorption of power with high rate is not cost-effective solution and lifetime limitation of the battery units is an important challenge of [38], [41], the contribution of battery units in inertia response is not possible in real [42], [43]. Therefore, utilizing of HES units for providing inertial response and primary frequency control required to considerer the ramp rate of output power limitation with minimum possible capacity [44]–[46].

The previous researches worked out have different challenges. To categorize the challenges clearly, Table. 1 summarises inertia response techniques challenges. It should mention that the effect of the phase-locked loop (PLL) on frequency control is also another challenge that is not in our paper scope [47].

In addition to all the challenges that are discussed, delays in the measurement and transmission of the signal are another challenge of power grid stability. For the stable performance of MG, a real-time balance between demand and generation must be established so that the frequency remains constant in allowable frequency limits [48]–[57]. The stability of the frequency control in the presence of time delay is investigated [58], [59], but these studies do not

TABLE 1. Inertia control techniques in high-penetrated wind generator grids and their challenges.

Inertia response techniques in high-penetrated wind generator grids	Contributions	Concerns
Deloading operation mode for the wind turbines [20-28].	Adaptive the deloading ratio [23]	This method requires the wind speed which is not practical to be measured especially in wind farms
	Analytical method [24]	This method requires wind speed data and the saved characteristics of wind turbines.
	Tuning Drop controller parameters for low- and high- wind speeds in [26]	Dependency of the droop gains to the wind speed
	Complete frequency control scheme including deloading operation [27]	Controller gains are tuned with respect to the wind speed
	Based on Regulation of the pitch angle [25]	Not enough fast for inertia response
Methods based on releasing kinetic energies [29-36]	Improved power-rotor speed trajectory curves with using *df/dt* term[31-33]	An operation point, in which the mechanical and electrical powers are equal, must be determined. Thus, these methods implementation, due to wind speed variations and other mechanical and electrical uncertainties, in real systems is difficult.
	Stepwise inertia control [34, 35]	Relatively high second frequency nadir is the main drawback of this method. Due to low inertia of MGs, the second nadir may impose very large disturbance to MGs
	An improved step wise inertia control [36]	The wind turbine operation point must be settled on a point in which mechanical and electrical power must be equal. Therefore, this method cannot be implemented easily in real cases.
Integration of energy storages with renewable sources [37-41]	Integration of wind generator with ultra-capacitor [37, 39].	These papers do not give any solution to charge the ultra-capacitor to be ready to participate in case of successive frequency drop perturbations
	Coordination among the battery unit and multiple wind turbines to achieve [38]	The dynamic characteristics of the power sources must be known in this method. Also, the power and the rotor speed limitations of the wind turbines and the maximum allowable rate of the exchangeable power of the battery with the grid are not considered.
	Covering Second frequency nadir challenge by superconducting magnetic energy storage (SMES) unit integrated with the wind farm [40].	This paper dose does not optimize the capacity of the SMES unit to achieve a cost-effective approach.
	Increasing the wind power penetration with considering battery capacity is proposed in [41].	The ramp rates of batteries, guarantee sufficient SOC of the batteries for continuous contribution in frequency control and control techniques are not notified

consider wind power participation in frequency behaviour improvement.

According to the aforementioned discussions about the challenges, Fig. 1 illustrates the research gaps and highlights the related contributions. Also, the process derivation of the proposed ideas of this paper is shown in Fig. 1. According to this Figure, this paper attempts to improve the inertia response of the MG using virtual inertia control of a wind unit in coordinated with a hybrid energy storage, which consists of ultra-capacitor and battery units. The *dp/dt* limitation of the wind unit, SOC control of the HES, and communication delay are considered in this study. Finally, the multi-objective optimization method determines the capacitance of ultra-capacitor, the contribution level of wind units in the inertial response, communication system delay, and the values of the controller coefficients to minimize the operation cost of MG operation and frequency oscillation.

II. VIRTUAL INERTIAL CONCEPT OF WIND GENERATOR

In this paper, two power sources are used to participate in increasing the virtual inertia of the studied MG.

- Wind generators: High kinetic energy can be released to the grid and reduces power imbalance in the grid.
- Energy storage sources: different energy storage sources are necessary for each MG to store or release energy. These sources can participate in frequency damping in the MGs.

A. THE CAPABILITY OF WIND GENERATORS IN INERTIAL SUPPORT

Wind generators output powers can be regulated by controlling the power electronics interfaces. On the other hand, the available kinetic energy in the wind turbine can provide inertia response to MGs. Therefore, wind power generators can participate in MGs frequency damping when a high disturbance occurs in the MG.

The wind generator output power depends on different factors such as air density ρ, Rotor diameter R, and wind speed υ_ω [23]–[28].

$$p_w = \frac{1}{2}\rho\pi R^2 \upsilon_\omega^3 \tag{1}$$

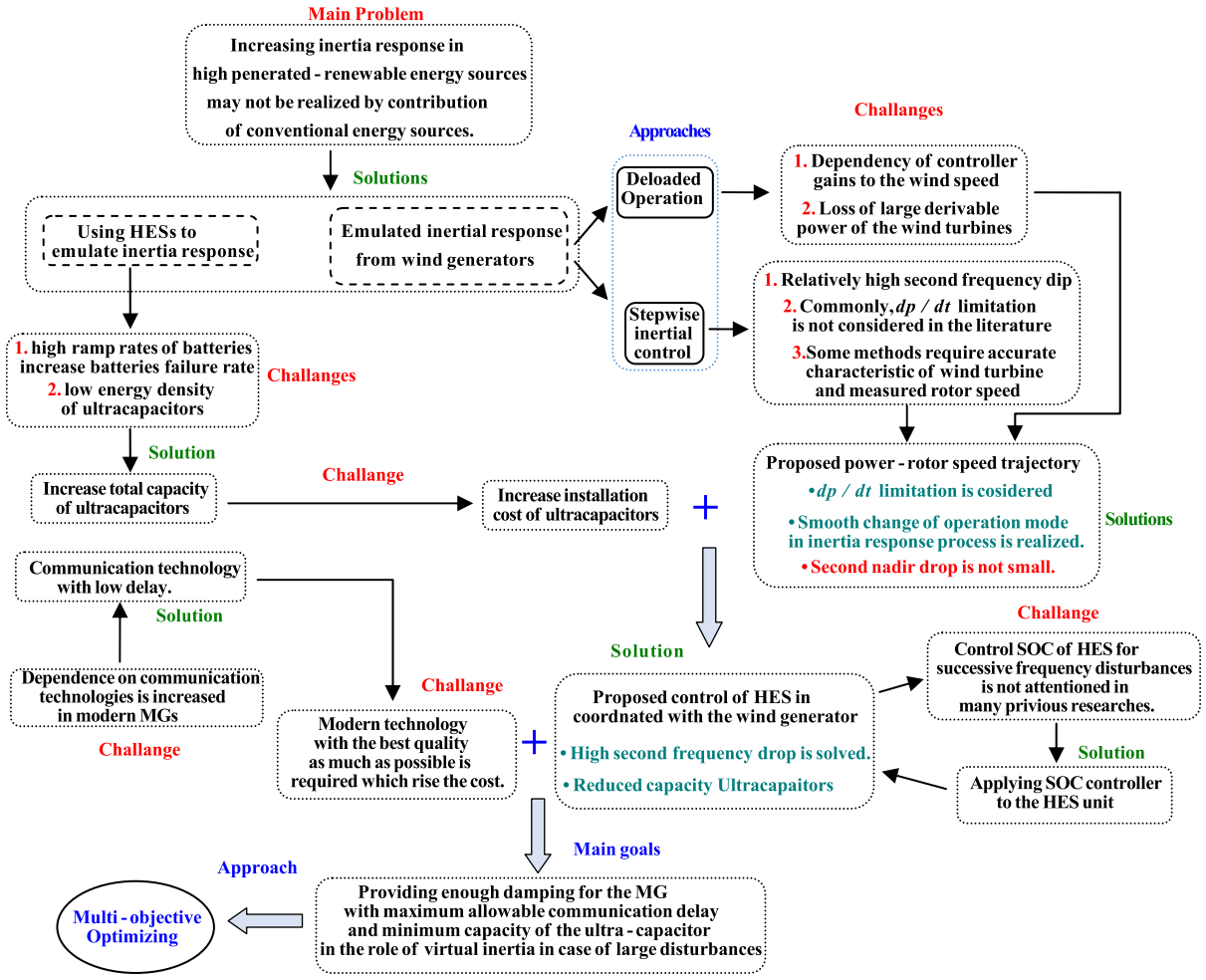

FIGURE 1. Derivation process of the different approaches considering challenges of pervious works.

It is not possible to convert all energy into electricity. The total power generated by the wind turbine can be calculated as follows,

$$P_m = \frac{1}{2}\rho\pi R^2 \upsilon_\omega^3 C_p(\lambda, \beta) \tag{2}$$

In the above equation, the factor $C_p(\lambda, \beta)$ depends on the design of the turbine, the pitch angle β and the tip-speed ratio λ.

$$\begin{cases} P_m = \frac{1}{2}\rho\pi R^2 \upsilon_\omega^3 C_p(\lambda, \beta) \\ \lambda = \omega_r R/\upsilon_\omega \end{cases} \tag{3}$$

where ω_r is the angular velocity of the wind turbine. Considering a constant value for β, the maximum power point (MPP) can be derived for different wind speeds as shown in Fig. 2.

To implement a cost-effective wind generator, the wind turbines are recommended to operate under MPPT conditions. These conditions can be approximated as a simple function that is shown in Fig. 2. To operate the wind turbine under maximum power point tracking (MPPT), deloaded operation strategy is not employed, thus the wind turbine participates in inertial response only [23]–[28].

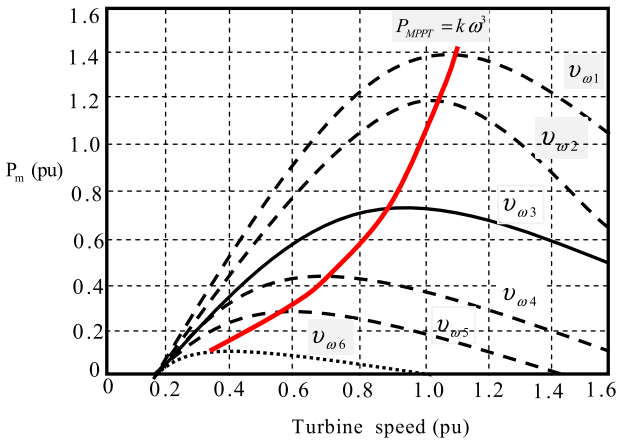

FIGURE 2. Aerodynamic characteristics of a wind turbine for different wind speeds.

MGs are targeted to feed by a high penetration level of renewable energy sources which have low inertia. In these grids, when a sudden high-power unbalancing occurs, severe frequency oscillation maybe not damped effectively.

Thus, many power sources or loads may be isolated from the grid by opening protection relays. With continuing this

situation, the blackout phenomenon is inevitable. For a limited time, to improve the inertial response of the grid, the wind generators can release more power over of MPP. Releasing the kinetic energy of the wind turbine causes to reduce wind rotor speed.

In a MG consisting of grid-connected generator units, the net power disturbance is in result of sudden changes in power generation (ΔP_G) or load consumption (ΔP_L). The frequency deviation function is depending on the net power disturbance ($\Delta P_G - \Delta P_L$), the MG inertia value and frequency dependant load coefficient (D) as seen in follows [12]–[16], [21]–[23], [25], [60], and [61]:

$$\Delta f(s) = \frac{\Delta P_G(s) - \Delta P_L(s)}{\frac{2H_s}{f_{sys}}s + D} \tag{4}$$

Due to applying new grid codes to MGs, the wind generators are required to inject more power to the MGs to prevent high frequency drops. Increasing the inertia of the MGs in cases of load disturbances is an alternative solution. Increasing the inertia response of the MGs causes to reduce the rate of change of frequency (*ROCOF*). With decreasing *ROCOF*, other power sources have enough time to increase their output power to compensate the unbalance of active power. Thus the frequency nadir would be decreased significantly. The *ROCOF* can be calculated as follow:

$$\Delta f(s) = \frac{0 - \frac{\Delta P_L}{s}}{\frac{2H_s}{f_{sys}}s + D} \tag{5}$$

$$ROCOF = \frac{d(\Delta f(t))}{dt}_{t=0^+} = \frac{-\Delta P_L}{\frac{2H_s}{f_{sys}}} \tag{6}$$

If a power source can inject future power to the grid with respect to the $\frac{d(\Delta f(t))}{dt}$ at the load disturbance moment, the inertia of the MG increases for transient states.

$$\Delta f(s) = \frac{K_i s\Delta f(s) - \frac{\Delta P_L}{s}}{\frac{2H_s}{f_{sys}}s + D} \tag{7}$$

$$ROCOF = \frac{d(\Delta f(t))}{dt}_{t=0^+} = \frac{-\Delta P_L}{\frac{2H_s}{f_{sys}} + K_i} = \frac{-\Delta P_L}{\frac{2(H_s+H_{vir})}{f_{sys}}} \tag{8}$$

where, K_i is the inertial gain of the system. Also, $K_i = 2H_{vir}/f_{sys}$. Considering (8), with increasing the inertia of the MG, *ROCOF* decreases. Thus the inertia control adjusts the power output of a wind turbine based on the *ROCOF* of the power system. To adjust the inertia response of the wind generator, the reference signal (P_{ref_wind}) for the wind generator should be summation the MPP power reference (P_{MPPT}) and inertia power reference ($P_{Vir\_H\_wind} = K_i\frac{d^2f}{dt^2}$) as follow:

$$P_{ref\_wind} = P_{MPPT} + K_i\frac{d^2f}{dt^2} \tag{9}$$

Considering the previous equations, it can be found that to implement virtual inertia; a derivative term in controllers of the power sources must be used. In practical applications, using a derivative controller might bring the risk of noise amplification for higher values of controller gain. Thus, using different filtering methods are reported by the previous researches [45], [46]. In this paper, a low-pass filter is used for the Ultracapacitor to suppress the noise and very low-frequency disturbances. Also, in this paper, two deadbands, which can reduce the effect of noise on the used controller operation [47] are used to prevent power wind generators to react against small frequency fluctuations.

More details of mathematical modelling for wind turbines' synthetic inertia can be found in the literatures [11], [32], [34], and [35] which are not discussed in this paper to prevent the expression of redundant and duplicate content. According to the literature reports, the dp/dt value of the wind generator should be limited to reduce mechanical stress of wind turbines [60]. Thus, the $P_{Vir\_H\_wind}$ and P_{wind} can be rewritten as follow:

$$\frac{dP_{Vir\_H\_wind}}{dt} \leq \left(\frac{dp}{dt}\right)_{\max} \tag{10}$$

$$P_{wind} \leq \left\{\left(\frac{dp}{dt}\right)_{\max} \times t + P_{MPPT}\right\} \tag{11}$$

In the literature, different recovery stages are presented [29]–[36]. In the recovering process, the operating region of a wind generation must be considered, which is investigated appropriately in few papers. The mentioned region limits the released kinetic energy to the grid and shortage duration time of the wind generator participating in inertia response. The maximum power, torque limitation, low and high-speed limitations are effective factors in the maximum available kinetic energy. These limitations are determined by green lines that shown in Fig. 3.

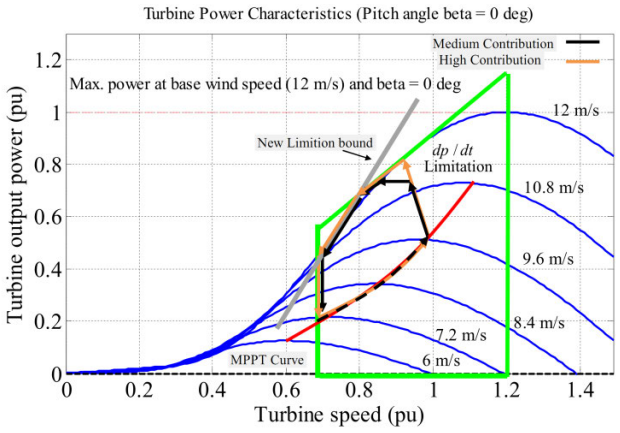

FIGURE 3. The proposed Inertia control process of a wind turbine with the defined limitations.

Besides the mentioned limitations, a new limitation bound, which is shown with gray line in Fig. 3 is considered in this paper to reduce the sudden power decreasing amplitude in changing operation stage. Upon issuance of command from the controller after detecting severe frequency drop, the output power increases suddenly. According to the literature reports, the dp/dt value of the wind generator in sudden

increasing power mode duration its contribution in inertia response should be limited to reduce mechanical stress of wind turbines [60]. This limitation is also considered in the proposed power-rotor speed trajectory.

The wind generator output power depends on wind speed υ_ω. For high υ_ω, the operation point of the wind turbine trajectory automatically reaches a point in which the mechanical and electrical power is equal. When the wind turbine operates that point, the wind turbine power and the rotor speed remain constant until the time duration of the wind turbine contribution in inertia response reach the end (t_{max}) and after that, the operation mode of the wind turbine changes to the MPPT mode. An example of operational features of the proposed strategy scheme for high wind speed is shown in Fig. 4. As seen in this figure, when the operation point of the wind turbine reaches $A_4(\mathrm{P_A}, \omega_{\mathrm{rA}})$, the mechanical and electrical power equals and the operating point of the turbine will remain constant at this point until time duration of the wind reach t_{max}. Then, the wind turbine operation mode changed to the MPPT mode and the wind power dropped suddenly.

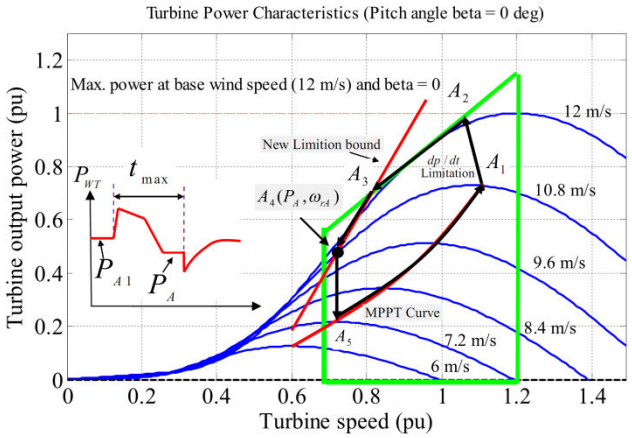

FIGURE 4. Contribution of the wind turbine in inertia control for high wind speed.

Two criterions are considered to terminate the contribution of the wind generator in inertia response. When the rotor speed of the wind turbine reaches the critical value of the desired time duration of the wind energy generation which participates in inertia response is over, the output power falls suddenly and the system mode is changed to MPPT mode. With applying conventional stepwise inertia control, the magnitude of ΔP_{off} is high and may lead the MG to unstable operation condition or causes a non-acceptable frequency dropping. Thus, using the capability of wind generators in inertia response faces serious challenges. To solve this problem, firstly, the power-rotor speed trajectory is modified in this paper as seen in Fig. 4. Second step is utilizing extra power storage units with high dynamic response must be employed. Motivated by the mentioned challenges, this paper proposes using power storage units in coordinated with inertia response of wind generators to improve the frequency recovery of the MG.

III. POWER STORAGE UNITS PARTICIPATING IN INCREASING THE INERTIA CONSTANT OF MG

Among power storage units, batteries and Ultra-capacitors have good characteristics for integration into the MGs, which would give the MGs active and effective capability to improve frequency recovery while sudden disturbances occur. Ultra-capacitors are good candidates for releasing or observing high power support in the milliseconds to seconds' time scales. Batteries can support the grid for more time scales. These storage units should co-operate together to solve the challenge of wind generators participating in inertial response.

A. PROPOSED HES COORDINATION STRATEGY WITH WIND TURBINE OPERATION

Ultra-capacitors can inject/absorb power with high *dp/dt* and so they can be employed to improve the inertia response of MGs. Due to their fast dynamic response in charging and discharging, these equipments can emulate inertia response of synchronous energy sources in MGs. But ultra-capacitors have low energy density. On the other hand, with development in battery technologies, the batteries are cost-effective with high storing energy capability. Therewith, batteries can be used widely in MGs to keep the power balance between power sources and load power consumption. Meanwhile, employing batteries to handle low power peaks is not recommended, because lifetime of the batteries may be damaged significantly [42], [43]. Therefore, batteries can be good candidates just for participating in primary and secondary frequency supports. With increasing the penetration of renewable energy sources in the MGs, the energy storage units may not support suddenly transient load demands, thus the frequency would drop with high rate (high *df/dt*). To solve this problem, the contribution of wind generators to improve frequency is necessary. Also, a new strategy to control the output power of energy storage devices and wind turbine should be applied.

Fig. 5 shows the proposed strategy steps mentioned above. The schematic diagram of the ultra-capacitor, battery and grid-connected inverter are shown in Fig. 5(a). The output power profiles of the mentioned subsystems versus the time are shown in Fig. 5 (b). The mentioned steps discussed in this section can be distinguished in Fig. 5 (b). The main task of the proposed ultra-capacitor-battery hybrid system which is coordination with the wind generator inertia response. It should be mentioned that when a large disturbance occurs to the MG, high *df/dt* imposed on the MG, thus the frequency-based controller of the wind generator issues the command of kinetic energy releasing at $t = t_{on}$. Therefore, ton is a time that high *df/dt* appearances. When the wind generator changes it operation mode to the MPPT mode, $t = t_{off}$ can be obtained.

With consideration of the mentioned discussions and Fig. 5, the proposed strategy steps can be presented as follow:

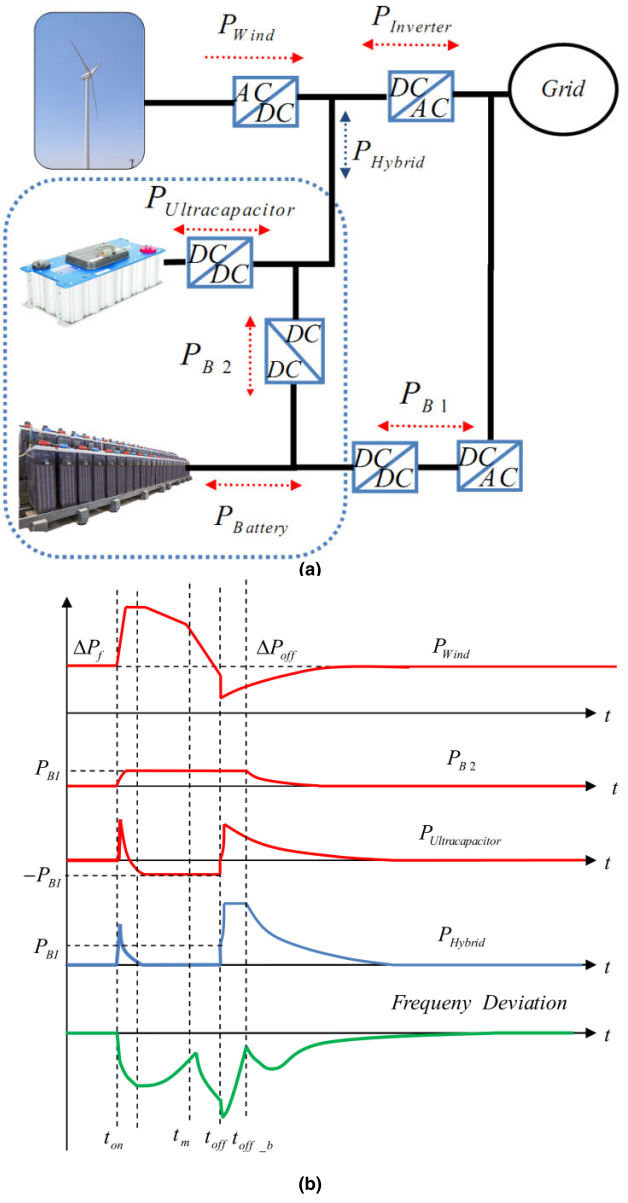

FIGURE 5. The coordination HES systems with the wind generator, (a): Schematic diagram of the energy storage systems with the wind generator, (b): Output power profile of the energy storage systems and the wind generator.

• The Ultra-capacitor can act immediately, but the battery bank can act after a delay [42], [43]. Thus, at first, wind turbine and the Ultra-capacitor should participate in the inertia response of studied MG to solve high *df/dt* challenge.

• While the wind turbine injects its kinetic energy to the grid, the battery power should set at a suitable level (P_{BI}). The P_{BI} value can be calculated according to the maximum power limitation of the battery and the ΔP_{off}. The generated power by the battery (P_{B2}) must be absorbed by the Ultra-capacitor to increase the SOC of the Ultra-capacitor which was reduced due to its participation in inertia response at $t = t_{on}$. When the operation mode of the wind turbines changes at $t = t_{off}$, the P_{B2} immediately can be completely transferred to the common inverter to supply the grid. With employing this strategy, the battery is kept be ready to act as an additional inertia source to reduce the second nadir due to the operation change of the wind turbine. The output summation powers of the energy storage devices can compensate wind power drop ΔP_{off}

• Also, when the operation point of the wind turbine meets the new limitation bound ($t = t_m$), the battery can inject power to grid to compensate the power dropping of the wind turbine. Since the reference power of the common inverter must be set with respect to the operation point trajectory of the wind turbine, the reference power for regulation $P_B(\omega_r)$ can be calculated easily.

• When large load disturbance occurs, the frequency drops with high *df/dt*. The wind generator injects some portion of its kinetic energy to the grid, thus the df/dt reduces. When the output powers of the energy sources reach certain values, the frequency recovered. Since the wind generator power is higher than the MPPT power, the summation of the output power of other energy sources is less than the load power. With decreasing the wind turbine power at the operation mode changing moment, the frequency drops suddenly and the second frequency nadir occurs. But applying the coordinated strategy between the wind and HSE unit, the frequency is recovered. When the operation of the HES unit comes back to the normal operation mode, the third nadir frequency occurs. Secondary and primary controllers of the power sources cause to compensate the third frequency nadir smoothly.

In MGs, power sources are commonly distributed in the grids. But there are high potentials for equipping the MGs with communication links. In cases that the energy storage units are far from the wind farms, it is possible to coordinate the power profiles of the storage unit with the power-rotor speed trajectory of the wind farm through communication links. The rotor speed of the wind turbine, the link dc voltage, the power reference of the inverter, t_{on} and t_{off} can be transmitted through the communication link to controller unit of the HES as shown in Fig. 6.

B. PROPOSED HES CONTROL SCHEME

In the HES unit, the Ultra-capacitor and battery units are integrated to provide high power density and high energy density features simultaneously. Each storage device is controlled by its own controller. In this section, the controllers' structures of the Ultra-capacitor and battery units are described.

Fig. 7 shows the block diagram controller of the Ultra-capacitor. To participate in inertia response of MG, the power reference of the Ultra-capacitor unit must have a term which is depended on df/dt as follow:

$$P_{\mathrm{Vir}} = -2H_{Vir}\frac{df}{dt} \tag{12}$$

In the above equation, P_{Vir}, H_{Vir}, and df/dt are the virtual power contribution of the Ultra-capacitor, the virtual inertia value and frequency derivative, respectively.

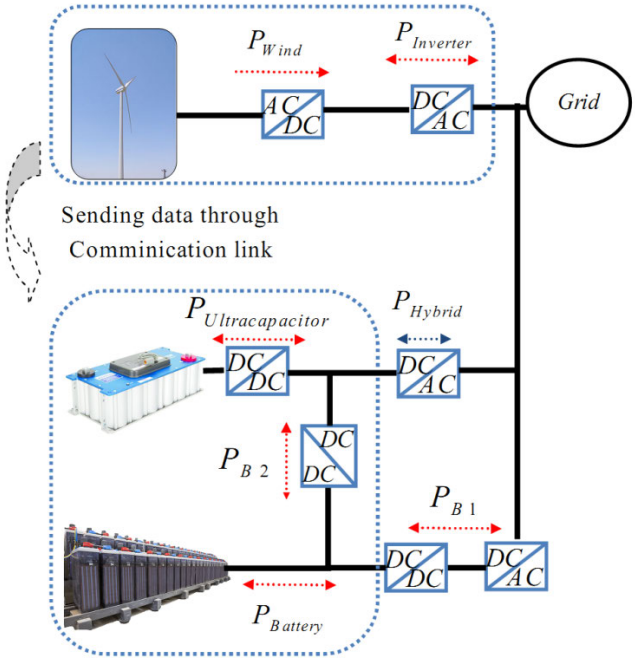

FIGURE 6. Information exchange link diagram of the HES unit and the wind generator.

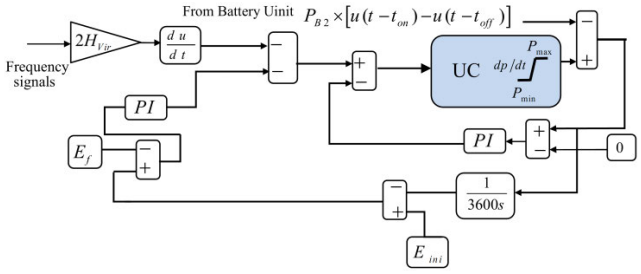

FIGURE 7. Block diagram of the Ultra-capacitor unit controller.

When the rotor speed is close to the wind turbine critical speed or the participation time of the wind turbine is coming to end, the suddenly wind turbine power can be estimated (ΔP_{old}) as follow:

$$\Delta P_{off} = P_{WT}|_{t=t_{off}\ \text{or}\ \omega_r=\omega_{critical}} - P_{\text{MPPT}} \tag{13}$$

where, $P_{\text{MPPT}} = k\omega_r^3$ (see Fig.1).

Due to contribution of The Ultra-capacitor unit in reduce the second nadir and inertia response; its stored energy may reach to a critical level. Thus, the SOC of the Ultra-capacitor unit is monitored and it is targeted to be fixed on a certain value. As seen in Fig. 5, the Ultra-capacitor unit absorbs the P_{B2} duration t_{on} and t_{off} which is shown in Fig. 7. Also, the net power transferred from the Ultra-capacitor unit must be set zero to guarantee capability of the Ultra-capacitor unit to handle the transient of subsequent disturbances. Two PI controllers can do the mentioned tasks appropriately as seen in Fig. 7. In this figure, the SOC of the Ultracapacitor is monitored and compared to the reference SOC to apply to a PI controller. Thus, the sufficient SOC of the Ultracapacitor can be guaranteed during simulation. Also, to prevent the contribution of the Ultracapacitor in generation power in steady-state conditions, another PI controller is used. Thus the steady-state reference power is set zero.

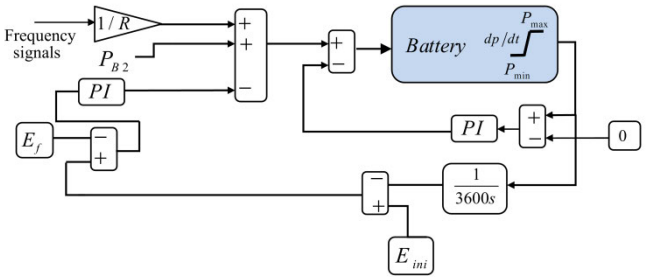

FIGURE 8. Block diagram of the battery unit controller.

Fig. 8 shows the block diagram controller of the battery unit. To participate in primary frequency, the power reference of the battery unit must have a term which is depended on Δf as follow:

$$P_{PB} = \frac{\Delta f}{R} \tag{14}$$

where P_{PB}, Δf and R are the contribution level of the battery in primary frequency control, the frequency deviations and droop coefficient of the battery.

To generate the signal P_{B2}, the maximum power of the battery and the maximum ΔP_{off} (i.e. $\Delta P_{off-\max}$) should be considered. The $\Delta P_{off-\max}$ can be calculated with respect to the wind turbine characteristic and the defined limitation (see Fig. 3). The maximum value of the P_{B2} (i.e. P_{BI}) can be determined as follow:

$$P_{BI} = P_{B\max} - \Delta P_{off-\max} \tag{15}$$

Thus, the signal P_{B2} can be generated according to the proposed strategy (See Fig. 5(b)) and Eq. (8) as seen as follows:

$$\begin{aligned} P_{B2} = {} & P_{BI}\left[u(t-t_{on}) - u(t-t_{off})\right] \\ & + P_{BI}\left[u(t-t_{off}) - u(t-t_{off\_b})\right] \end{aligned} \tag{16}$$

where $t_{off\_b} - t_{off} = \alpha$. With employing this strategy, the difference between the time of sudden drop of wind turbine power and the power drop of auxiliary converter of the battery will be sufficient. Thus, the occurrence of high secondary frequency drop will be eliminated.

As the battery unit do many tasks duration of the wind turbine contribution in frequency support, the SOC of the battery may reach to the critical level. A PI controller is used to stabilize the SOC of the battery. Also, the net power transferred from energy storages is controlled by another PI controller to set zero reference for the battery power in the steady state condition. These targets are seen in Eq.10.

$$\begin{cases} \int_{t=0}^{t=t_{sim}} \Delta P_B = 0 \\ E_B(t)_{(t\to\infty)} = E_f \end{cases} \tag{17}$$

where, ΔP_B, E_B, and E_f, are output power oscillation of the battery system (pu), the saved energy in the battery system (pu), and the final reference power (pu), respectively.

It should mention that PI controllers which are used to maintain the SOC of super-capacitor and battery at the desired value don't limit their capability to maintain the stability of system frequency and power when facing continuous disturbances, it seems that there are contradictions in maintaining constant SOC of hybrid energy storing system and the stability of system frequency as well as its power output. However, the PI controllers control the SOC and the net power of these devices slowly and the primary frequency responses of the hybrid energy storage provide faster and more robust performance.

IV. THE STUDIED MG

In this paper, an islanded MG system is considered as a case study. A wind energy penetrated MG is considered. The MG consists of production units, storage devices and telecommunication infrastructures. Diesel generator, fuel cell, solar system and wind unit are responsible to generate power. The electrolyser unit is also used to absorb excess power. A HES device consists of an ultra-capacitor and battery units is employed in this MG. An ultra-capacitor unit is used to generate or rapidly absorb the power, aims to increase the virtual inertia of the grid. The battery is responsible to support the primary or secondary control. The PV penetration level is considered low and the PV unit works under MPPT mode for all the time. The batteries and other power sources will participate in primary and secondary frequency response to eliminate the frequency steady state error.

A. THE MG CENTRAL CONTROLLER

In the studied MG, secondary control orders are set by a central control base. The central controller requires grid frequency and unbalancing power value information to properly command the power generation and the electrolyser units. Theses main measured parameters are transmitted by the telecommunications platform with a certain delay time, which is very effective on the stability of the MG. The studied MG block diagram is illustrated in Figure 9. As discussed in the literature such as [11], [25], and [44], first-order and second order models for diesel generator and other sources are well-known and acceptable models for investigating the frequency area. Also, to simulate the behaviour of the wind unit for frequency analyses, a model consists of aerodynamic characteristic, mechanical and electrical model can be used. A Detail of each source model is shown in Fig. 9. Except diesel generator, the power sources units are connected to the grid by power electronic interfaces which are used to convert the generated power to AC power from DC sources such as solar panels, fuel cells, and storage equipment.

Primary and secondary controllers are employed to damp frequency oscillation. Each power source has its own unique droop characteristic. This characteristic is shown as an R coefficient in the frequency-related feedback block.

The primary controller controls the power exchange of the power units around the operating point for small load changes. When a large disturbance occurs, the central control unit faces steady-state frequency deviation. Therefore, a secondary controller is required as a supplementary controller to adjust the new operation point of all power sources. In secondary control, the central control unit monitors the frequency and power fluctuations. Frequency fluctuation is multiplied by bias coefficient (B) and power fluctuation signal. Then, they apply to a PI controller in the central control unit to regulate the new operation point for each power source unit.

B. OPTIMIZATION DETAILS

In this paper, it is assumed the Ultra-capacitor capacity as an additional inertia source is employed. With increasing its capacity, the inertia response of the MG improves [61] but, the cost of the installed Ultra capacitor increases significantly [62]. In case of using the Ultra-capacitor for emulating the inertial response, relationship between its capacity and virtual inertia should be determined. In this regard, detail equations are discussed in [61]. It can be concluded that there is a linear relationship between the virtual inertia value and the capacitance of the Ultra-capacitor. High virtual inertia values are obtained with selecting high capacity Ultra-capacitors. Thus, the value of H_{Vir} determines the capacity of the Ultra-capacitor.

Less communication delay means high communication services quality and thus it cost more [63]. Thus, damping frequency oscillations with consideration communication delay as high as possible is an interesting objective. It means cheap communication infrastructure is required for the MG.

For low ultra-capacitor capacity and the high delay value of telecommunication systems, the operation cost would be low. These two parameters are integrated in one objective function and shown in following Equation:

$$F_1 = \frac{H_{Vir}}{H_{Virm}} + \frac{T_{dc}}{T_d} \tag{18}$$

The communication system delay and the average acceptable delay the simulation process are notated with T_d, and T_{dc} respectively. Also, H_{Virm} is the average virtual inertia. Selecting high values for H_{Virm} means that the high capacity ultra-capacitor can be chosen. Different values for H_{Virm} can be selected depending on the maximum allowable capacity for the ultra-capacitor. For example, in [47], the minimum and maximum inertia values are zero and 0.2 (pu/Hs) respectively. Thus, H_{Virm} is 0.1 (s) in this paper to conduct optimization and analyses. The values considered for communication delay in the presented studies (<0.5s) are realistic for a small microgrid where the length of communication links is short [63], and [64]. In this paper, T_{dc} is 0.2 (s) as the weight factor of the fitness functions.

The main aim of this paper is to reduce the frequency oscillation of the MG. Equation (11) shows one of the fitness functions. As wind turbine and the Ultra-capacitor should

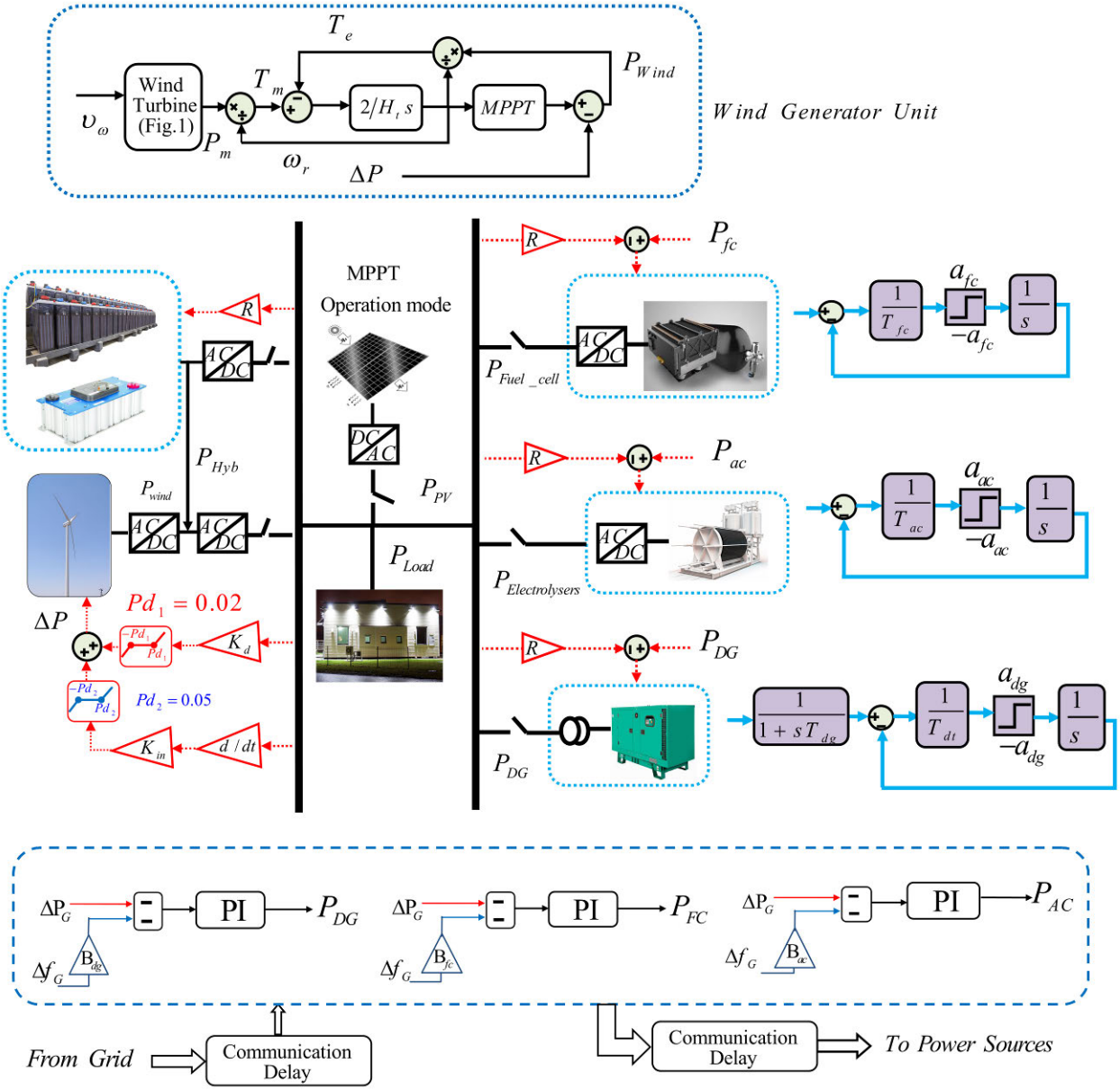

FIGURE 9. Block diagram of the MG with the central control unit based on the sources models reported in [11], [25], [44], [55], [65]–[68].

participate in the inertia response of studied MG to solve high *df/dt* challenge, *df/dt* in the optimization of the control parameters must be considered. Also, keeping the frequency in desirable range [0.95-1.05] pu has a specific importance. Thus, a penalty factor (ρ) is applied to the second objective function.

$$IAE_{V_{wk}} = \begin{cases} \rho \times \sum_{i=1}^{N} |\Delta f|_i \times t_i \\ \qquad \left| {}^{df}/_{dt} > k_{\max} \right| or\ |\Delta f| > 0.05^{pu} \\ \sum_{i=1}^{N} |\Delta f|_i \times t_i \\ \qquad else \end{cases}$$

$$F_2 = \sum_{k=8.5} IAE_{V_{wk}} \tag{19}$$

where, $IAE_{V_{wk}}$ is the integral absolute error of The MG frequency when the wind speed is k (m/s). t_i is simulation time step.

In this paper, $\rho = 10$ and $k_{\max} = 0.4$ are considered. By using NSGA-II algorithm, equation (19) is attempted to be minimized so that frequency recovery will be improved. In this paper, 16 coefficients are targeted to be found by NSGA-II algorithm to minimize the Eq. (18) and (19) simultaneously. These coefficients are listed in Table. 2.

V. SIMULATION RESULTS

To implement the MG, MATLAB/ SIMULINK software is used. As reported in the literature [55], [65]–[67], first-order

TABLE 2. The controllers and main parameters limitation ranges.

Parameter	Limitation	Parameter	Limitation
H_{Vir}	[0.05-0.3]	kp_{ac}	[0.4-8]
kp_{dg}	[0.03125-0.0625]	ki_{ac}	[.01-0.5]
ki_{dg}	[0.1-5]	B_{ac}	[0.08-0.2]
B_{dg}	[5-12]	R_{ac}	[10-20]
R_{dg}	[.025-0.05]	R_b	[0.07-.75]
k_{pfc}	[0.5-1]	T_d	[0.02-.5]
ki_{fc}	[.04-.016]	K_{in}	[.1-.45]
R_{fc}	[8-15]	k_d	[.1-.45]

TABLE 3. MG constant parameters.

Parameter	Value	Parameter	Value
T_{uc}	0.05 (s)	f_{base}	50/60 Hz
H	12 (s)	K_{power_b}	0.09
D	0.01/0.012 (pu/Hz)	K_{lower_b}	0.11
T_{dg}	2 (s)	K_{power_U}	0.095
T_{FC}	2 (s)	K_{lower_U}	0.105
T_{AC}	0.1 (s)	$K_{pcharge\_b}$	0.1
T_{dt}	2.5 (s)	$K_{Icharge\_b}$	0.05
f_{base}	50 Hz	$K_{pcharge\_U}$	20
T_{dt}	2.5 (s)	$K_{Icharge\_U}$	0.5

dynamic models for the fuel-cell, the diesel generator, the electrolyser, the battery and the ultra-capacitor have sufficient accuracy to simulate dynamic response in frequency deviation analyses. Also, a low order model of the wind generator consists of the aerodynamic characteristic wind turbine, the mechanical part and MPPT unit [68] can be used in the frequency analysis of MGs. The feasibility of the proposed strategy discussed in previous sections with considering nominal parameters given in Table 3; is shown through simulation results. In this paper, two scenarios for participating the power sources in load frequency control are investigated. In the first scenario, the frequency of the grid with and without employing the proposed strategies is investigated. In the following, the optimized parameters that are tuned with NSGA-II algorithm are employed. Then, the obtained results are compared.

A. SCENARIO I: CONTRIBUTION OF THE HES AND WIND TURBINE GENERATOR IN INERTIA CONTROL

Firstly, the MG is simulated with and without wind turbine contribution in inertia response. In this step, the coordination operation of the wind turbine and the HES is not applied in the simulation. The non-optimum parameters for simulation in this first scenario are listed in Table. 4.

The wind speed is 9.5 m/s. The wind-turbine characteristic is shown in Fig. 2. The MG is in the steady state before t = 500(s). At t = 500(s), the load changes suddenly and cause to high *df/dt* as seen in Fig. 10. *The df/dt* value is 0.571 Hz/s in this case. The frequency is dropped suddenly. But with using the capability of the wind turbine in inertia response, the *df/dt* is reduced (0.4 Hz/s) and the maximum frequency drop is reduced effectively. But, when the operation mode of

TABLE 4. The non-optimum Parameters for the first scenario.

Parameter	Value	Parameter	Value
H_{Vir}	0.2	kp_{ac}	06275
kp_{dg}	1.791	ki_{ac}	0.4
ki_{dg}	0.24	B_{ac}	0.1
B_{dg}	0.1687	R_{ac}	16.1
R_{dg}	8.542	R_b	0.3571
k_{pfc}	0.764	T_d	0, 0.02, 0.05
ki_{fc}	0.1	K_{in}	0.41
R_{fc}	12.7212	k_d	0.2

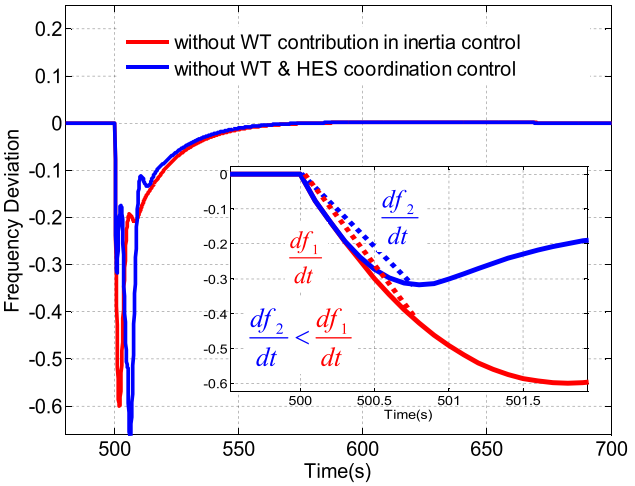

FIGURE 10. Frequency of the MG in Scenario I, without coordination operation the wind turbine and the HES unit under 9.5 *m/s* wind speed.

the wind turbine changes, due to the sudden power drop of the wind turbine, high power disturbance is imposed on the MG and the second nadir frequency appears which is higher than the first frequency nadir. Therefore, the contributions of wind turbines in the MGs, due to the low inertia of the MGs, are not recommended without any additional resourcefulness. The necessity coordination of the HES with the wind generator for improving the frequency response of grid is highlighted in Fig. 9.

In the second step, the MG is simulated with applying the coordinated operation schema of the wind turbine with the HES unit in inertia response. The frequency of the MG is shown in the Fig. 11. The second nadir is reduced effectively. While the wind turbine injects its kinetic energy to the grid, the second dc/dc converter which is connected to the battery (see Fig. 4) smoothly increase its output power (P_{B2}) up to the P_{BI} value. Before $t = t_{off}$, this additional power of the battery is absorbed by the Ultracapacitor. When the operation mode of the wind turbine changes, the P_{B2} immediately is completely transferred to the grid to compensate the second frequency nadir. With employing this strategy, the battery is kept be ready to act as an additional inertia source to reduce the second nadir due to the operation change of the wind turbine. When the duration time of participation of the battery unit in inertia control frequency reach the end, the P_{B2}

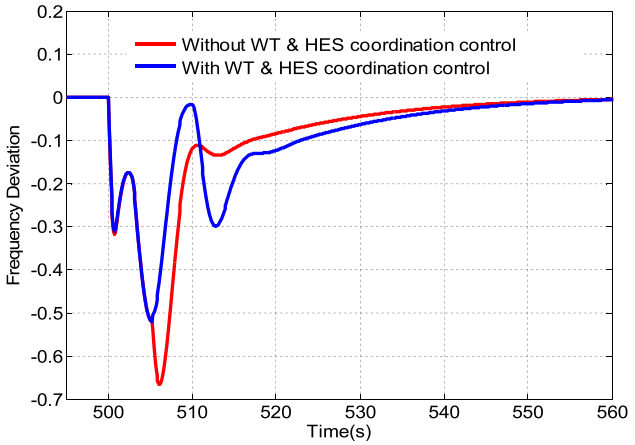

FIGURE 11. Frequency of the MG in Scenario I, with and without coordinated operation the wind turbine and the HES unit under 9.5 m/s wind speed.

reduced smoothly. But the third frequency nadir is imposed to the MG. However, the third frequency nadir is not critical.

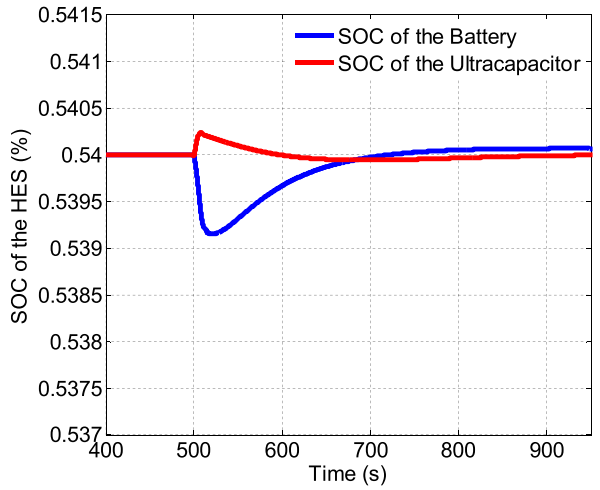

FIGURE 12. SOC profiles of: the Ultracapacitor and the battery.

It should notify that the SOC of the battery and the Ultracapacitor changes suddenly duration their coordinated operation with the wind turbine. But the mentioned SOC controllers can regulate their SOC at the desirable level. The SOC of the Ultracapacitor is shown in Fig. 12. Since the Ultracapacitor is charged by the P_{B2}, the SOC of the Ultra-capacitor is increased duration of coordinated operation the wind turbine and the HES unit. After this duration, The SOC controller regulates the SOC of the Ultracapacitor smoothly. Also, the SOC of the battery is shown in Fig. 12.

The battery unit contribute in primary frequency control and inject the P_{B2} to the MG for the specific time, thus the SOC of the battery reduced. But the SOC of the battery comes back to the initial value by using the PI controller. As discussed in here, with employing the SOC controllers, the HES unit kept ready to participate effectively for the next

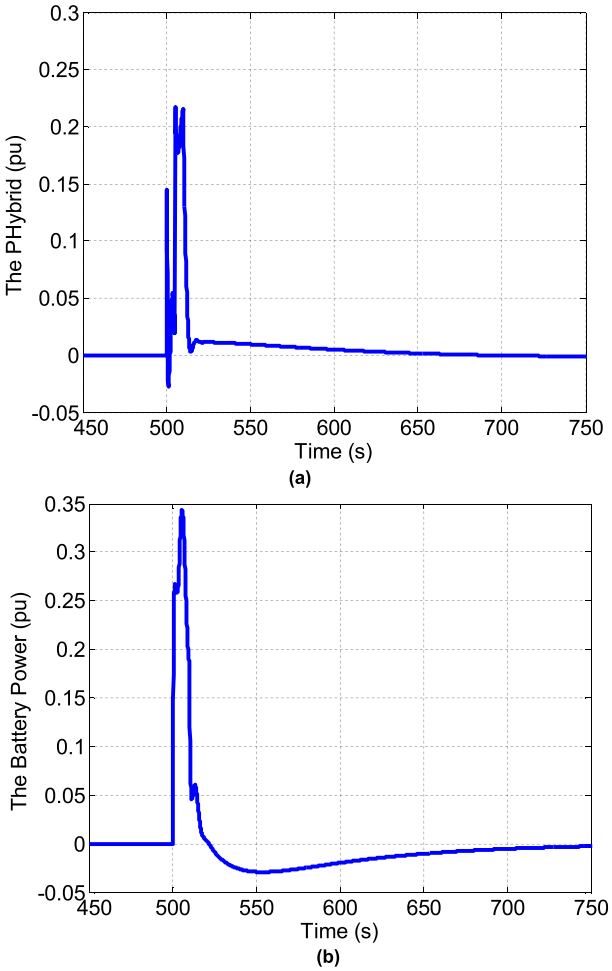

FIGURE 13. The HES output power versus time: (*a*) : the Ultracapacitor output power, (*b*) the battery output power under 9.5 *m*/*s* wind speed.

events. Also, the net exchanged power of the Ultra-capacitor and battery units is set on zero value. Thus, the HES unit just participate in transient response of the MG to reduce the frequency deviation. The output power of the energy storages is shown in Fig. 13. As seen in this Figure, the net exchanged power of the energy storages with the MG was at the zero level. After t = 500 (s), these devices inject power to the grid and then the output powers of them are going toward zero. Therefore, the output power controllers of the HES unit have successful feasibility.

The impact of the wind turbine operation point on the capability of wind generators in inertial support should be investigated. In the third step, the capability of the wind turbine in inertia response and its effect on the MG frequency response for different wind speed is investigated. The Virtual inertia capability of the wind turbine is closely related to operation range of wind turbines. Therefore, the power-rotor speed trajectories, the wind generator output power and the MG frequency deviation for different wind speed are derived and shown in the Figs. 14-16, respectively.

When the rotor speed reaches the critical speed (ω_{cr} = 0.72p.u), the operation mode changing is enabled

and the wind generator operation mode come back to the MPPT mode. Also, for high wind speed, the time duration of the wind turbine contribution in inertia response may be higher than $t_{max}(= 10(s))$, therefore, the rotor speed of the wind generator may be higher than the critical speed at the changing operation mode time.

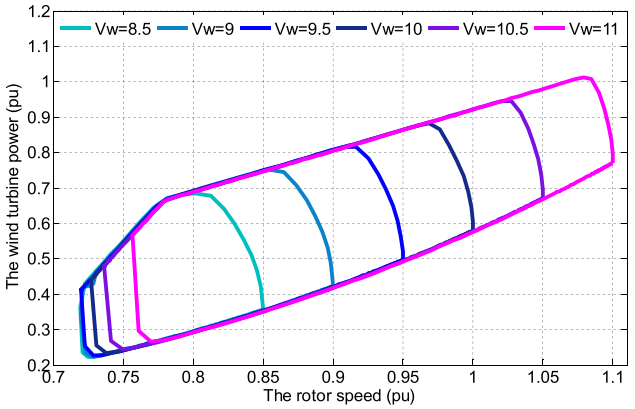

FIGURE 14. Operational characteristics of the wind turbine in inertia emulation schemes for different wind speed.

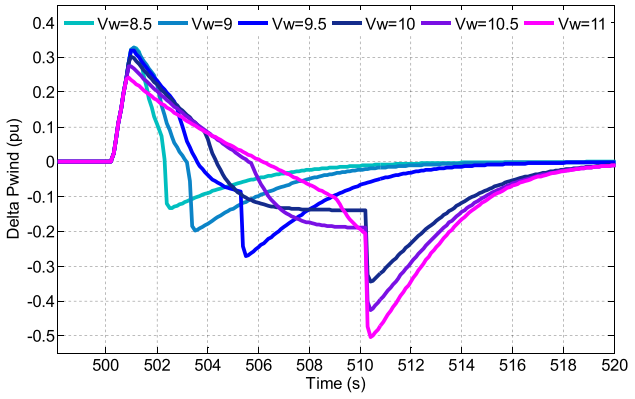

FIGURE 15. The wind generator output power in inertia emulation schemes for different wind speed.

With respect to the Fig. 14 and Fig.15, time duration of contribution of the wind generator in releasing its kinetic energy increases. Reducing the first nadir with employing inertia response of the wind turbine by increasing the wind speed is observed in Fig. 16. But, for high wind speed ($>= V_w = 10.5$/s), the amplitude of instantaneous increase in wind generator power for improving system inertia is low. Thus the first frequency nadir is increased. Due to t_{max} limitation, the operation mode changing of the wind turbine is realized before the ω_{cr} for high wind speed. Thus, the $\Delta P_{off-\max}$ is increasing with increasing the wind speed and as a result, the second frequency nadir is increased as seen in Fig. 16. Higher first and second frequency nadir for the conditions that the wind speeds are high; are results of applying the mechanical and electrical limitations to the wind generators. But time duration of the wind generator in

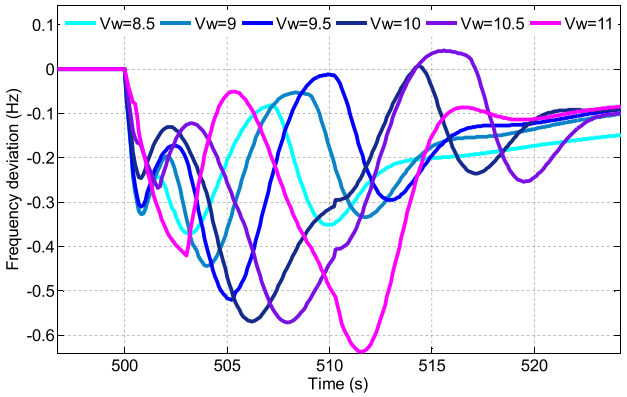

FIGURE 16. The MG frequency response with considering inertia response of the wind turbine for different wind speed.

inertia response is high for high wind speeds. Thus the other power sources can increase their output as more as possible to reduce the second nadir. Selection proper parameters of the controllers can be solved this challenge significantly. An optimizing approach is described in the 4.2 section.

To reduce the first and second frequency drops as much as possible, the capacity of the Ultracapacitor can be increased. But the installation cost of the Ultracapacitor increases significantly.

In the fourth step, employing the wind turbine in the primary frequency control is investigated. The wind turbine controller is equipped with drooped controller as shown in Fig. 8. With employing the drooped controller, the primary frequency response of the MG can be improved. Thus the tertiary frequency nadir is expected to be reduced. Fig. 17 shows the impact of employing drooped controller of the wind generator on the frequency deviation of the MG. When the operation mode of the wind generator changes, the frequency deviation is reduced as shown Fig.17.

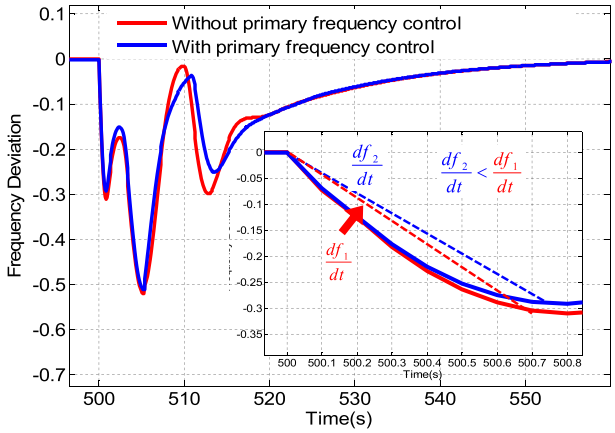

FIGURE 17. The frequency response of the MG with employing drooped control of wind turbine under 9.5 m/s wind speed.

In fifth step, to illustrate the effect of delays on the MG frequency response, three sets of communication are considered as seen in Fig. 18. The power sources and loads data

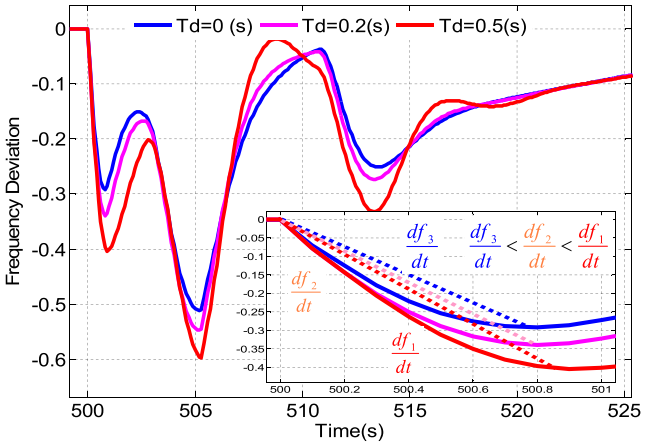

FIGURE 18. Frequency responses of the MG for different communication delays.

are transmitted to the central controller and local controller through communication delay. With increasing the communication delay, the frequency deviation increases. Thus, the communication delay time should be reduced as much as possible. By using the advanced communication infrastructure, the communication delay would be reduced but the operation cost increases. Therefore, trade of the operation cost and frequency deviation should be done by the MG operator. Fig. 18 shows that the first, second and third frequency nadirs increase with increasing the time delay.

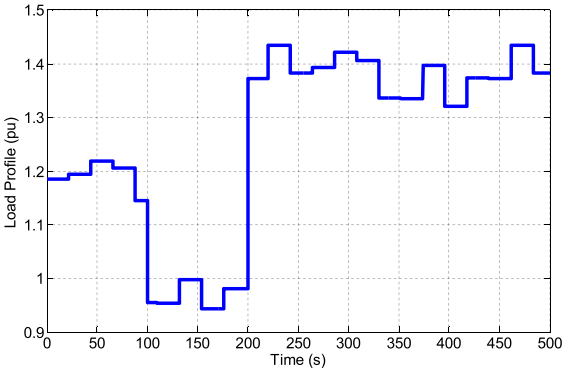

FIGURE 19. Stochastic load profile.

B. SCENARIO: APPLYING OPTIMUM PARAMETERS FOR THE CONTROLLERS

In this section, the different parameters of the controllers are obtained through multi objective optimizing algorithm and consideration stochastic load and PV power profiles for different wind speeds. The step changes pattern of the load profile and PV output power follow normal and beta distribution [69] as shown in Fig. 19 and Fig. 20, respectively. As discussed in Eq. 19, the simulation setup must be run for different wind speed cases to calculate the final second fitness function. Thus, for multi-objective optimization, the wind speed is increased step by step to cover all wind speed possibilities. In this section, Maximum wind speed is Vw = 10.5 (m/s). Thus, with respect to the Fig. 3, the maximum wind generator output power is 0.67 (pu).

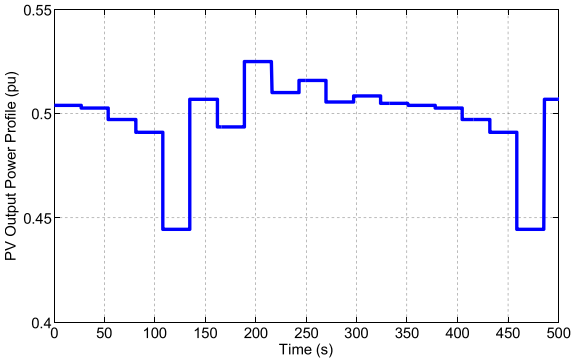

FIGURE 20. Stochastic output power profile of PV.

It should mention that the employed optimizing algorithm is just used to remove the complexity of the parameters tuning. The main aim of this section is showing impact of optimized parameters on operation cost (F1) reduction and improved frequency deviation of the MG, simultaneously. At the end of the optimizing process, the final Pareto solution points are obtained as shown in Fig. 21. As seen in this figure, different solutions can be selected. To have a minimum oscillation frequency with minimum operation cost, a middle point can be selected as seen in Fig. 21.

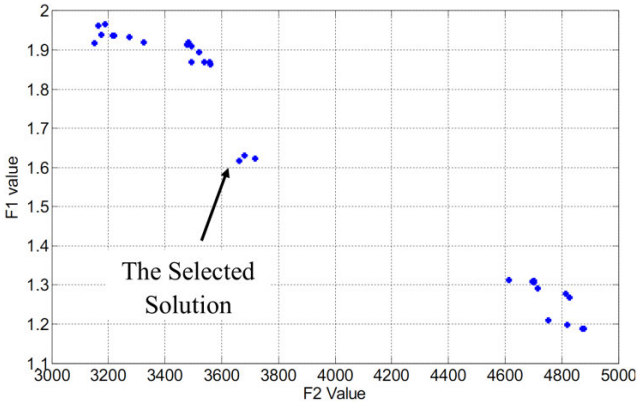

FIGURE 21. Frontiers of Pareto of the two objective functions driven from NSGA-II optimization.

The obtained results for the selected solution are listed in Table 5. To show the effectiveness of selected solution in overcoming frequency drops and overshoots, the system is simulated, and the obtained results compare with a non-optimum base strategy.

Fig. 22 shows this comparison and effectiveness of the proposed strategy with optimized parameters. Frequency overshoots, nadirs and settling times are reduced effectively with employing the optimum parameters. The fitness functions values are listed in Table. 5. By employing optimum parameters, the F1 value which is related to the operation cost of the

TABLE 5. The optimum parameters.

Parameter	Non-Optimum Value	Optimum Value	Parameter	Non-Optimum Value	Optimum Value
H_{Vir}	0.2	0.1134	kp_{ac}	0.6275	0.458
kp_{dg}	0.18	0.1633	ki_{ac}	0.4	0.4605
ki_{dg}	0.24	0.32	B_{ac}	0.4	0.1922
B_{dg}	0.1687	0.14	R_{ac}	16.1	19.72
R_{dg}	8.54	7.8	R_b	0.357	0.209
k_{pfc}	0.764	0.905	T_d	0.5	0.48
ki_{fc}	0.1	0.136	K_{in}	.413	0.49
R_{fc}	12.721	11.1425	k_d	0.2	0.36
F1	2.4050	1.6175	**F2**	4240	3662

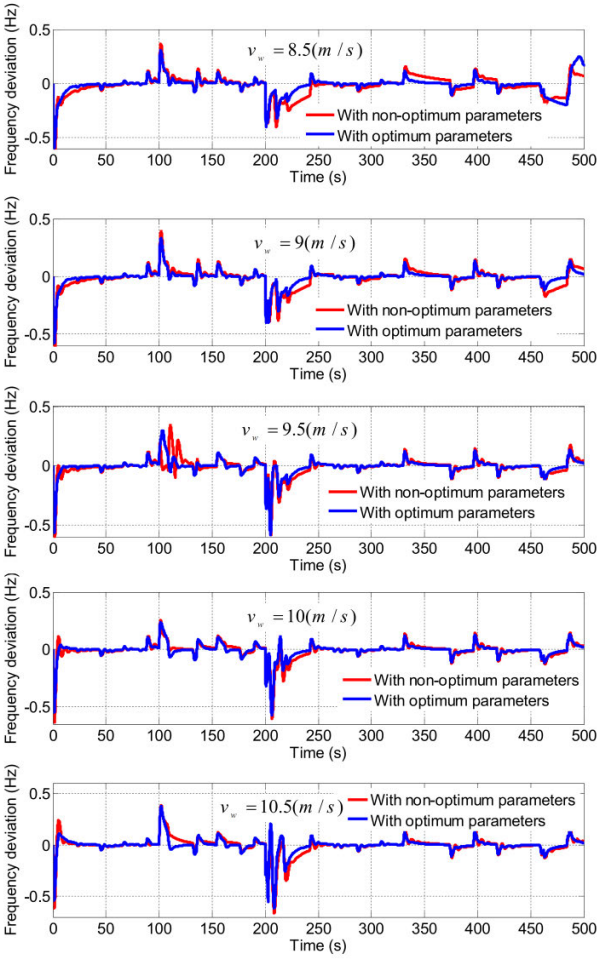

FIGURE 22. Frequency deviation with optimum and non-optimum parameters.

MG decreases. Since the Ultracapacitor capacity is reduced for the selected optimum solution, the installation cost of the Ultra-capacitor is expected to reduce significantly [61], [62]. Also, the F2 value reduction indicates that the overall frequency deviation of the MG for different wind speeds, are reduced.

To prove the controller of HES unit, simulation results of SOC of energy storages when facing continuous disturbances are shown in Fig. 23. This figure is just presented when the wind speed is 8.5(m/s).

C. STUDYING FREQUENCY DEVIATIONS WITH RESPECT TO THE GRID CODES

When the MG frequency is outside of the desired range, the power sources can tolerate this situation for the specific time ranges. If the frequency of the MG cannot come back to the normal conditions quickly, the power sources would be isolated from the MG, and cascade tripping events may be occurred and this has the potential to MG blackouts in worst conditions.

It is important to note that the simulation results show that the maximum MG frequency deviation and maximum *df/dt* is well compatible with different standards in the presence of load perturbations and different wind speeds. In this section, different grid codes are considered to investigate the capability of the implemented control system in overcoming the frequency deviations challenges. Some simulation results are shown in Fig. 24. The maximum Δf and *df/dt* of the MG are reported in Table. 6. This table information is used to show that the frequency can deviations of the MG meet the different standards. Some grid codes are listed ad follow:

TABLE 6. The MG response to load disturbances with/without wind contribution in frequency support.

Scenarios	Clearing time Δf	SRM ?	Clearing time *df/dt*	SRM ?
With wind generator contribution in frequency support	Δf <-0.7 Hz ≈0(s)	Yes	*df/dt* >0.5 Hz/s *max(df/dt)=0.53* Hz/s ≈0.9 (s)	Yes
Without wind generator contribution in frequency support	Δf <-0.7 Hz ≈1.36(s)	No	*df/dt* >0.5 Hz/s *max(df/dt)=0.63* Hz/s ≈1.2 (s)	No

SRM: Standards requirements have been met?
Clearing time *Δf*: it is the time between the start time for frequency deviation to go lower than the allowable frequency and the time to return to normal frequency conditions.
Clearing time *df/dt*: the time between the start time for *df/dt* exceeding the allowable limit and the time to return to normal conditions.

- **IEEE Std 929-2000**: This standard allow the PV units to be connected to the grid just for six cycle for a conditions that the frequency deviation is beyond +0.833% or −1.166%.
- **IEEE Std 1547-2003:** This standard offered to set the under-frequency relay according to the defined "clearing time". If the frequency deviation is beyond +0.833% or −1.166%, the distributed sources can be connected within 0.16 (s).
- **df/dt Std:** df/dt standards vary in different country. The Irish (Ausgrid/ EvoEnergy), Great Britain (National Grid), and Australian National Electricity Market (NEM) *df/dt* standard cite a minimum access standard of 1Hz/s for 1 second [70], [71].

Due to the contribution of the wind generator in frequency regulation, the maximum frequency drops values are lower

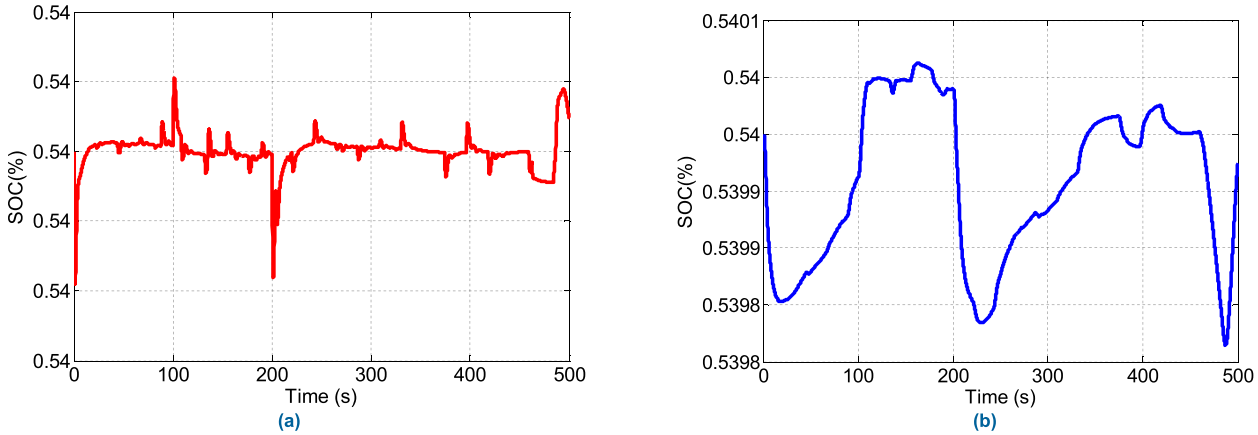

FIGURE 23. Simulation result of SOC of (*a*) : The Ultracapacitor and (*b*) : battery during simulation time for υ_ω =8.5(m/s).

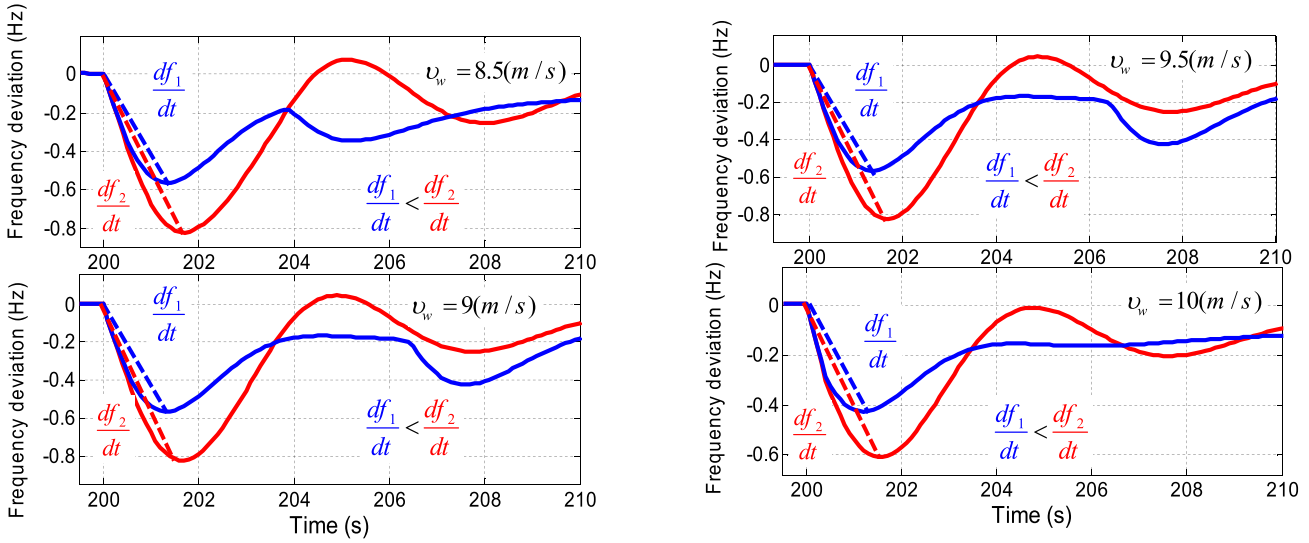

FIGURE 24. Frequency of the MG in with (blue curves) and without (red curves)the proposed strategy under different wind speeds.

than the 0.7 (Hz). Thus the frequency oscillation amplitudes are in limited ranges which are advised by the standards. Simulation results have indicated that the *df/dt* values due to different response of power sources to the load disturbances may be greater than 0.5Hz/s. But time duration of abnormal *df/dt* conditions are not high and met different *df/dt* standards.

VI. CONCLUSION

In this paper, a new control strategy is proposed to control the operation of the HES unit in coordinated with the inertia response of the wind generator in MGs. It is shown that employing coordination of wind generators with HES could improve the frequency stability of low inertia MGs in severe disturbance conditions. The HES consists of a battery and an Ultra-capacitor bank, which is connected to a common DC link. In this paper, a wind energy penetrated MG is considered. Therefore, it can participate in frequency regulation. When a frequency event occurs, the wind turbine immediately injects incremental power and participates in stepwise inertial control. Simultaneously, the ultra-capacitor is discharged to boost the inertial response, coordinated with the wind turbine. The battery and Ultra-capacitor kept ready to inject maximum power after the wind turbine's operating mode changing. As the HES should not supply or absorb power for a long time, two control loops for the hybrid storage system is used to keep the available energy of the HES at the desirable level. Simulation results show the feasibility of the proposed coordination strategy to overcome high frequency drops challenged and the reducing the second frequency nadir due to the contribution of the wind turbine in inertia response.

Also, a central control unit is used to determine the contribution levels of different power sources in the frequency recovery process. The power sources are connected to the central control with communication links that impose a delay between sending and receiving ordered signals. Obviously, with increasing the Ultra-capacitor capacitance and decreasing communication delay, frequency oscillation damping enhances but the operation cost of the grid increases. To implement a satisfactory frequency damping in versus of power disturbances in the MG and reduces operation cost,

the controller parameters, the contribution level of the wind generator in inertia response, and the virtual inertia value are tuned by the NSGA-II algorithm. The simulation results with optimum parameters.

Also, the frequency oscillations are investigated in different Grid Codes points of view. The frequency behaviour of the MG can meet the requirements of the studied standards. Applying optimized parameters to the controllers, considering *dp/dt* limitation to the wind generator, employing the Ultracapacitor with as low as possible capacity and the communication infrastructure with as high as possible delay which allows the MG to satisfy the grid code but do not impact seriously the wind generator lifetime.

REFERENCES

[1] N. Hatziargyriou, *Microgrids: Architectures and Control*. Hoboken, NJ, USA: Wiley, 2014.
[2] J. Vasquez, J. Guerrero, J. Miret, M. Castilla, and L. Garcia de Vicuna, "Hierarchical control of intelligent microgrids," *IEEE Ind. Electron. Mag.*, vol. 4, no. 4, pp. 23–29, Dec. 2010, doi: 10.1109/MIE.2010.938720.
[3] N. Javaid, G. Hafeez, S. Iqbal, N. Alrajeh, M. S. Alabed, and M. Guizani, "Energy efficient integration of renewable energy sources in the smart grid for demand side management," *IEEE Access*, vol. 6, pp. 77077–77096, 2018, doi: 10.15302/J-ENG-2015099.
[4] M. Soshinskaya, W. H. J. Crijns-Graus, J. M. Guerrero, and J. C. Vasquez, "Microgrids: Experiences, barriers and success factors," *Renew. Sustain. Energy Rev.*, vol. 40, pp. 659–672, Dec. 2014, doi: 10.1016/j.rser.2014.07.198.
[5] C. Chen, J. Wang, F. Qiu, and D. Zhao, "Resilient distribution system by microgrids formation after natural disasters," *IEEE Trans. Smart Grid*, vol. 7, no. 2, pp. 958–966, Mar. 2016, doi: 10.1109/TSG.2015.2429653.
[6] Z. Abdmouleh, R. A. M. Alammari, and A. Gastli, "Review of policies encouraging renewable energy integration & best practices," *Renew. Sustain. Energy Rev.*, vol. 45, pp. 249–262, May 2015, doi: 10.1016/j.rser.2015.01.035.
[7] R. Lee, S. Homan, N. Mac Dowell, and S. Brown, "A closed-loop analysis of grid scale battery systems providing frequency response and reserve services in a variable inertia grid," *Appl. Energy*, vol. 236, pp. 961–972, Feb. 2019, doi: 10.1016/j.apenergy.2018.12.044.
[8] T. Rahimi, S. H. Hosseini, M. Sabahi, M. Abapour, and G. B. Gharehpetian, "Three-phase soft-switching-based interleaved boost converter with high reliability," *IET Power Electron.*, vol. 10, no. 3, pp. 377–386, Mar. 2017, doi: 10.1049/iet-pel.2016.0211.
[9] A. Ebrahimi and S. H. Fathi, "Optimisation of MG operation considering effects of power electronic converters," *IET Renew. Power Gener.*, vol. 13, no. 3, pp. 213–2021, 2019, doi: 10.1049/iet-rpg.2018.5605.
[10] S. Wei, Y. Zhou, and Y. Huang, "Synchronous motor-generator pair to enhance small signal and transient stability of power system with high penetration of renewable energy," *IEEE Access*, vol. 5, pp. 11505–11512, 2017, doi: 10.1109/ACCESS.2017.2716103.
[11] Y. Cheng, R. Azizipanah-Abarghooee, S. Azizi, L. Ding, and V. Terzija, "Smart frequency control in low inertia energy systems based on frequency response techniques: A review," *Appl. Energy*, vol. 279, Dec. 2020, Art. no. 115798, doi: 10.1016/j.apenergy.2020.115798.
[12] A. A. El-Fergany and M. A. El-Hameed, "Efficient frequency controllers for autonomous two-area hybrid microgrid system using social-spider optimiser," *IET Gener., Transmiss. Distrib.*, vol. 11, no. 3, pp. 637–648, Feb. 2017, doi: 10.1049/iet-gtd.2016.0455.
[13] T. Mahto and V. Mukherjee, "Fractional order fuzzy PID controller for wind energy-based hybrid power system using quasi-oppositional harmony search algorithm," *IET Gener., Transmiss. Distrib.*, vol. 11, no. 13, pp. 3299–3309, Sep. 2017, doi: 10.1049/iet-gtd.2016.1975.
[14] J. Tan and Y. Zhang, "Coordinated control strategy of a battery energy storage system to support a wind power plant providing multi-timescale frequency ancillary services," *IEEE Trans. Sustain. Energy*, vol. 8, no. 3, pp. 1140–1153, Jul. 2017, doi: 10.1109/TSTE.2017.2663334.
[15] U. Datta, A. Kalam, and J. Shi, "The relevance of large-scale battery energy storage (BES) application in providing primary frequency control with increased wind energy penetration," *J. Energy Storage*, vol. 23, pp. 9–18, Jun. 2019, doi: 10.1016/j.est.2019.02.013.
[16] J. W. Choi, S. Y. Heo, and M. K. Kim, "Hybrid operation strategy of wind energy storage system for power grid frequency regulation," *IET Gener., Transmiss. Distrib.*, vol. 10, no. 3, pp. 736–749, Feb. 2016, doi: 10.1049/iet-gtd.2015.0149.
[17] X. Hou, Y. Sun, X. Zhang, J. Lu, P. Wang, and J. M. Guerrero, "Improvement of frequency regulation in VSG-based AC microgrid via adaptive virtual inertia," *IEEE Trans. Power Electron.*, vol. 35, no. 2, pp. 1589–1602, Feb. 2020, doi: 10.1109/TPEL.2019.2923734.
[18] A. B. Attya, J. L. Dominguez-Garcia, and O. Anaya-Lara, "A review on frequency support provision by wind power plants: Current and future challenges," *Renew. Sustain. Energy Rev.*, vol. 81, pp. 2071–2087, Jan. 2018, doi: 10.1016/j.rser.2017.06.016.
[19] M. Dreidy, H. Mokhlis, and S. Mekhilef, "Inertia response and frequency control techniques for renewable energy sources: A review," *Renew. Sustain. Energy Rev.*, vol. 69, pp. 144–155, Mar. 2017, doi: 10.1016/j.rser.2017.06.016.
[20] Y. Fu, Y. Wang, and X. Zhang, "Integrated wind turbine controller with virtual inertia and primary frequency responses for grid dynamic frequency support," *IET Renew. Power Gener.*, vol. 11, no. 8, pp. 1129–1137, Jun. 2017, doi: 10.1049/iet-rpg.2016.0465.
[21] D. Ochoa and S. Martinez, "Fast-frequency response provided by DFIG-wind turbines and its impact on the grid," *IEEE Trans. Power Syst.*, vol. 32, no. 5, pp. 4002–4011, Sep. 2017, doi: 10.1109/TPWRS.2016.2636374.
[22] H. Ye, W. Pei, and Z. Qi, "Analytical modeling of inertial and droop responses from a wind farm for short-term frequency regulation in power systems," *IEEE Trans. Power Syst.*, vol. 31, no. 5, pp. 3414–3423, Sep. 2016, doi: 10.1109/TPWRS.2015.2490342.
[23] X. Bian, J. Zhang, Y. Ding, J. Zhao, Q. Zhou, and S. Lin, "Microgrid frequency regulation involving low-wind-speed wind turbine generators based on deep belief network," *IET Gener., Transmiss. Distrib.*, vol. 14, no. 11, pp. 2046–2054, Feb. 2020, doi: 10.1049/iet-gtd.2019.1161.
[24] R. Engleitner, A. Nied, M. S. M. Cavalca, and J. P. da Costa, "Dynamic analysis of small wind turbines frequency support capability in a low-power wind-diesel microgrid," *IEEE Trans. Ind. Appl.*, vol. 54, no. 1, pp. 102–111, Jan. 2018, doi: 10.1109/TIA.2017.2761833.
[25] V. Gholamrezaie, M. G. Dozein, H. Monsef, and B. Wu, "An optimal frequency control method through a dynamic load frequency control (LFC) model incorporating wind farm," *IEEE Syst. J.*, vol. 12, no. 1, pp. 392–401, Mar. 2018, doi: 10.1109/JSYST.2016.2563979.
[26] M. Fakhari Moghaddam Arani and Y. A.-R.-I. Mohamed, "Dynamic droop control for wind turbines participating in primary frequency regulation in microgrids," *IEEE Trans. Smart Grid*, vol. 9, no. 6, pp. 5742–5751, Nov. 2018, doi: 10.1109/TSG.2017.2696339.
[27] J. Zhao, X. Lyu, Y. Fu, X. Hu, and F. Li, "Coordinated microgrid frequency regulation based on DFIG variable coefficient using virtual inertia and primary frequency control," *IEEE Trans. Energy Convers.*, vol. 31, no. 3, pp. 833–845, Sep. 2016, doi: 10.1109/TEC.2016.2537539.
[28] D. Ochoa and S. Martinez, "Frequency dependent strategy for mitigating wind power fluctuations of a doubly-fed induction generator wind turbine based on virtual inertia control and blade pitch angle regulation," *Renew. Energy*, vol. 128, pp. 108–124, Dec. 2018, doi: 10.1016/j.renene.2018.05.047.
[29] J. Liu, Z. Yang, J. Yu, J. Huang, and W. Li, "Coordinated control parameter setting of DFIG wind farms with virtual inertia control," *Int. J. Electr. Power Energy Syst.*, vol. 122, Nov. 2020, Art. no. 106167, doi: 10.1016/j.ijepes.2020.106167.
[30] X. Wang, W. Gao, A. Scholbrock, E. Muljadi, V. Gevorgian, J. Wang, W. Yan, and H. Zhang, "Evaluation of different inertial control methods for variable-speed wind turbines simulated by fatigue, aerodynamic, structures and turbulence (FAST)," *IET Renew. Power Gener.*, vol. 11, no. 12, pp. 1534–1544, Oct. 2017, doi: 10.1049/iet-rpg.2017.0123.
[31] M. Kang, K. Kim, E. Muljadi, J. W. Park, and Y. C. Kang, "Frequency control support of a doubly-fed induction generator based on the torque limit," *IEEE Trans. Power Syst.*, vol. 31, no. 6, pp. 4575–4583, Nov. 2016, doi: 10.1109/TPWRS.2015.2514240.
[32] M. Kheshti, L. Ding, M. Nayeripour, X. Wang, and V. Terzija, "Active power support of wind turbines for grid frequency events using a reliable power reference scheme," *Renew. Energy*, vol. 139, pp. 1241–1254, Aug. 2019, doi: 10.1016/j.renene.2019.03.016.

[33] R. Azizipanah-Abarghooee, M. Malekpour, T. Dragicevic, F. Blaabjerg, and V. Terzija, "A linear inertial response emulation for variable speed wind turbines," *IEEE Trans. Power Syst.*, vol. 35, no. 2, pp. 1198–1208, Mar. 2020, doi: 10.1109/TPWRS.2019.2939411.

[34] M. Kheshti, L. Ding, W. Bao, M. Yin, Q. Wu, and V. Terzija, "Toward intelligent inertial frequency participation of wind farms for the grid frequency control," *IEEE Trans. Ind. Informat.*, vol. 16, no. 11, pp. 6772–6786, Nov. 2020, doi: 10.1109/TII.2019.2924662.

[35] W. Bao, L. Ding, Z. Liu, G. Zhu, and V. Terzija, "Analytically derived fixed termination time for stepwise inertial control of wind turbines—Part I: Analytical derivation," *Int. J. Electr. Power Energy Syst.*, vol. 121, Oct. 2020, Art. no. 106106, doi: 10.1016/j.ijepes.2020.106120.

[36] D. Yang, J. Lee, and Y. C. Kang, "Stepwise inertial control of a wind turbine generator to minimize a second frequency dip," *J. Int. Council Electr. Eng.*, vol. 6, no. 1, pp. 153–159, Jan. 2016, doi: 10.1080/22348972.2016.1202396.

[37] Arani and El-Saadany, "Implementing virtual inertia in DFIG-based wind power generation," *IEEE Trans. Power Syst.*, vol. 28, no. 2, pp. 1373–1384, May 2013, doi: 10.1109/TPWRS.2012.2207972.

[38] W. Bao, Q. Wu, L. Ding, S. Huang, F. Teng, and V. Terzija, "Synthetic inertial control of wind farm with BESS based on model predictive control," *IET Renew. Power Gener.*, vol. 14, no. 13, pp. 2447–2455, Oct. 2020, doi: 10.1049/iet-rpg.2019.0885.

[39] N. S. Hasan, N. Rosmin, N. M. Nordin, and M. Y. Hassan, "Virtual inertial support extraction using a super-capacitor for a wind-PMSG application," *IET Renew. Power Gener.*, vol. 13, no. 10, pp. 1802–1808, Jul. 2019, doi: 10.1049/iet-rpg.2018.5655.

[40] L. Miao, J. Wen, H. Xie, C. Yue, and W. J. Lee, "Coordinated control strategy of wind turbine generator and energy storage equipment for frequency support," in *Proc. IEEE Ind. Appl. Soc. Annu. Meeting*, May 2014, pp. 1–7, doi: 10.1109/TIA.2015.2394435.

[41] Y. Liu, W. Du, L. Xiao, H. Wang, and J. Cao, "A method for sizing energy storage system to increase wind penetration as limited by grid frequency deviations," *IEEE Trans. Power Syst.*, vol. 31, no. 1, pp. 729–737, Jan. 2016, doi: 10.1109/TPWRS.2015.2396528.

[42] J. Rocabert, R. Capo-Misut, R. S. Munoz-Aguilar, J. I. Candela, and P. Rodriguez, "Control of energy storage system integrating electrochemical batteries and supercapacitors for grid-connected applications," *IEEE Trans. Ind. Appl.*, vol. 55, no. 2, pp. 1853–1862, Mar. 2019, doi: 10.1109/TIA.2018.2873534.

[43] J. Fang, Y. Tang, H. Li, and X. Li, "A battery/ultracapacitor hybrid energy storage system for implementing the power management of virtual synchronous generators," *IEEE Trans. Power Electron.*, vol. 33, no. 4, pp. 2820–2824, Apr. 2018, doi: 10.1109/TPEL.2017.2759256.

[44] H. Mehrjerdi, E. Rakhshani, and A. Iqbal, "Substation expansion deferral by multi-objective battery storage scheduling ensuring minimum cost," *J. Energy Storage*, vol. 27, Feb. 2020, Art. no. 101119, doi: 10.1016/j.est.2019.101119.

[45] X. Shen, Z. Luo, J. Xiong, H. Liu, X. Lv, T. Tan, J. Zhang, Y. Wang, and Y. Dai, "Optimal hybrid energy storage system planning of community multi-energy system based on two-stage stochastic programming," *IEEE Access*, vol. 9, pp. 61035–61047, 2021, doi: 10.1109/ACCESS.2021.3074151.

[46] C. Zhang, E. Rakhshani, N. Veerakumar, J. L. R. Torres, and P. Palensky, "Modeling and optimal tuning of hybrid ESS supporting fast active power regulation of fully decoupled wind power generators," *IEEE Access*, vol. 9, pp. 46409–46421 2021, doi: 10.1109/ACCESS.2021.3066134.

[47] E. Rakhshani, A. Perilla, N. Veerakumar, Z. Ahmad, J. R. Torres, M. Meijden, and P. Palensky, "Analysis and tuning methodology of FAPI controllers for maximising the share of grid-connected wind generations," *IET Renew. Power Gener.*, vol. 14, no. 18, pp. 3816–3823, Feb. 2021, doi: 10.1049/iet-rpg.2019.1445.

[48] P. He, S. Arefifar, C. Li, F. Wen, Y. Ji, and Y. Tao, "Enhancing oscillation damping in an interconnected power system with integrated wind farms using unified power flow controller," *Energies*, vol. 12, no. 2, p. 322, Jan. 2019.

[49] B. Liu, T. Wu, Z. Liu, and J. Liu, "A small-AC-signal injection-based decentralized secondary frequency control for droop-controlled islanded microgrids," *IEEE Trans. Power Electron.*, vol. 35, no. 11, pp. 11634–11651, Nov. 2020, doi: 10.1109/tpel.2020.2983878.

[50] A. Fathi, Q. Shafiee, and H. Bevrani, "Robust frequency control of microgrids using an extended virtual synchronous generator," *IEEE Trans. Power Syst.*, vol. 33, no. 6, pp. 6289–6297, Nov. 2018, doi: 10.1109/TPWRS.2018.2850880.

[51] A. K. Barik and D. C. Das, "Expeditious frequency control of solar photovoltaic/biogas/biodiesel generator based isolated renewable microgrid using grasshopper optimisation algorithm," *IET Renew. Power Gener.*, vol. 12, no. 14, pp. 1659–1667, Oct. 2018, doi: 10.1049/iet-rpg.2018.5196.

[52] S. Kayalvizhi and D. M. Vinod Kumar, "Load frequency control of an isolated micro grid using fuzzy adaptive model predictive control," *IEEE Access*, vol. 5, pp. 16241–16251, 2017, doi: 10.1109/ACCESS.2017.2735545.

[53] J. Li, R. Xiong, Q. Yang, F. Liang, M. Zhang, and W. Yuan, "Design/test of a hybrid energy storage system for primary frequency control using a dynamic droop method in an isolated microgrid power system," *Appl. Energy*, vol. 201, pp. 257–269, Sep. 2017, doi: 10.1016/j.apenergy.2016.10.066

[54] C. Mu, Y. Zhang, H. Jia, and H. He, "Energy-storage-based intelligent frequency control of microgrid with stochastic model uncertainties," *IEEE Trans. Smart Grid*, vol. 11, no. 2, pp. 1748–1758, Mar. 2020, doi: 10.1109/TSG.2019.2942770.

[55] P. K. Ray and A. Mohanty, "A robust firefly–swarm hybrid optimization for frequency control in wind/PV/FC based microgrid," *Appl. Soft Comput.*, vol. 85, Dec. 2019, Art. no. 105823, doi: 10.1016/j.asoc.2019.105823.

[56] M. R. Chen, G. Q. Zeng, Y. X. Dai, K. D. Lu, and D. Q. Bi, "Fractional-order model predictive frequency control of an islanded microgrid," *Energies*, vol. 12, pp. 84–104, 2019, doi: 10.3390/en12010084.

[57] F. D. Mohammadi, H. K. Vanashi, and A. Feliachi, "State-space modeling, analysis, and distributed secondary frequency control of isolated microgrids," *IEEE Trans. Energy Convers.*, vol. 33, no. 1, pp. 155–165, Mar. 2018, doi: 10.1109/TEC.2017.2757012.

[58] G. A. Alizadeh, T. Rahimi, M. H. B. Nozadian, S. Padmanaban, and Z. Leonowicz, "Improving microgrid frequency regulation based on the virtual inertia concept while considering communication system delay," *Energies*, vol. 12, no. 10, p. 2016, May 2019, doi: 10.3390/en12102016.

[59] L. Jiang, W. Yao, Q. H. Wu, J. Y. Wen, and S. J. Cheng, "Delay-dependent stability for load frequency control with constant and time-varying delays," *IEEE Trans. Power Syst.*, vol. 27, no. 2, pp. 932–941, May 2012.

[60] Y. Wang, G. Delille, H. Bayem, X. Guillaud, and B. Francois, "High wind power penetration in isolated power systems—Assessment of wind inertial and primary frequency responses," *IEEE Trans. Power Syst.*, vol. 28, no. 3, pp. 2412–2420, Aug. 2013, doi: 10.1109/TPWRS.2013.2240466.

[61] M. Hajiakbari Fini and M. E. Hamedani Golshan, "Determining optimal virtual inertia and frequency control parameters to preserve the frequency stability in islanded microgrids with high penetration of renewables," *Electr. Power Syst. Res.*, vol. 154, pp. 13–22, Jan. 2018, doi: 10.1016/j.epsr.2017.08.007.

[62] H. Wang, T. Wang, X. Xie, Z. Ling, G. Gao, and X. Dong, "Optimal capacity configuration of a hybrid energy storage system for an isolated microgrid using quantum-behaved particle swarm optimization," *Energies*, vol. 11, no. 2, pp. 454–468, Feb. 2018, doi:10.3390/en11020454

[63] Z. Zhang, D. Dey, and Y. Tan, "Pricing communication services with delay guarantee," *Informs J. Comput.*, vol. 19, no. 2, pp. 248–260, May 2007, doi: 10.1287/ijoc.1050.0159.

[64] S. Liu, X. Wang, and P. X. Liu, "Impact of communication delays on secondary frequency control in an islanded microgrid," *IEEE Trans. Ind. Electron.*, vol. 62, no. 4, pp. 2021–2031, Apr. 2015, doi: 10.1109/TIE.2014.2367456.

[65] S. Mishra, G. Mallesham, and A. N. Jha, "Design of controller and communication for frequency regulation of a smart microgrid," *IET Renew. Power Gener.*, vol. 6, no. 4, pp. 248–258, Jul. 2012, doi: 10.1049/iet-rpg.2011.0165

[66] M.-H. Khooban, "Secondary load frequency control of time-delay standalone microgrids with electric vehicles," *IEEE Trans. Ind. Electron.*, vol. 65, no. 9, pp. 7416–7422, Sep. 2018, doi: 10.1109/TIE.2017.2784385.

[67] A. Latif, S. M. S. Hussain, D. C. Das, and T. S. Ustun, "Double stage controller optimization for load frequency stabilization in hybrid wind-ocean wave energy based maritime microgrid system," *Appl. Energy*, vol. 282, Jan. 2021, Art. no. 116171, doi: 10.1016/j.apenergy.2020.116171.

[68] J. Dai, Y. Tang, Q. Wang, and P. Jiang, "Aggregation frequency response modeling for wind power plants with primary frequency regulation service," *IEEE Access*, vol. 7, pp. 108561–108570, 2019, doi: 10.1109/ACCESS.2019.2933141.

[69] K. P. Kumar and B. Saravanan, "Recent techniques to model uncertainties in power generation from renewable energy sources and loads in microgrids – a review," *Renew. Sustain. Energy Rev.*, vol. 71, pp. 348–358, May 2017, doi: 10.1016/j.rser.2016.12.063.

[70] *Understanding ROCOF Protection*. Accessed: Feb. 2019. [Online]. Available: https://www.nojapower.com.au/images/Understanding%20ROCOF.pdf
[71] AEM Operator. (2016). *International Review of Frequency Control Adaptation*. [Online]. Available: https://www.aemo.com.au//media/Files/Electricity/NEM/SecurityandReliability/Reports/2016/FPSS-International-Review-ofFrequency-Control.pdf

TOHID RAHIMI (Member, IEEE) was born in Salmas, Iran. He received the B.Sc. degree from the University of Tabriz, Tabriz, Iran, in 2011, the M.Sc. degree in electrical engineering, in 2013, and the Ph.D. degree in system and power electronics from the University of Tabriz, in 2018. He was a Teacher Assistant duration his Ph.D. course at the University of Tabriz. He was a Supervisor or an Advisor of several M.Sc. Thesis at the Meraj Higher Education Institute, Iran. He is currently a Postdoctoral Researcher with Shandong University, Jinan, China. His research interests include power electronics, reliability, EMI, and different fields of power engineering. He has been served as an Active Reviewer for different IEEE and other scientific journals. Moreover, he won a competitive grant awarded by the China Postdoctoral Science Foundation, in 2020.

LEI DING (Senior Member, IEEE) received the B.E. and Ph.D. degrees in electrical engineering from Shandong University, Jinan, China, in 2001 and 2007, respectively. From 2008 to 2009, he was a Postdoctoral Researcher with Tsinghua University, Beijing, China. From 2010 to 2011, he was a Research Associate with The University of Manchester. He is currently a Professor with the School of Electrical Engineering, Shandong University. His research interests include power system wide-area protection, low inertia systems, and integration of renewable energy.

MOSTAFA KHESHTI (Member, IEEE) was born in Iran. He received the B.Sc. degree in control engineering from the Shiraz University of Technology, Iran, and the M.Sc. and Ph.D. degrees (Hons.) in power system engineering with Full Scholarships from Xi'an Jiaotong University, China, in 2013 and 2017, respectively. He has worked as a System Operator with the Regional Dispatching Center, Fars Regional Electric Company. He joined Shandong University, where he currently works as an Associate Professor. His research interests include low inertia systems, stability control and optimization of renewable energy integrated power systems using system identification, and computational intelligence methods. He was a recipient of the Shandong University Future Young Scholars Program, China.

RASOUL FARAJI (Member, IEEE) received the Ph.D. degree in electronics from the Department of Electrical and Computer Engineering, Isfahan University of Technology, Isfahan, Iran, in 2019. He was doing part of the Ph.D. dissertation with the École Polytechnique Fédérale de Lausanne (EPFL), Lausanne, Switzerland, as a Visiting Student. Since 2019, he has been a Postdoctoral Researcher with Shandong University, Jinan, China. His research interests include dc–dc switching converters, data analysis using artificial intelligence, implementing algorithms on FPGA, and integrated circuits design. He was a recipient of the Distinguished Researcher Award from the Graduate University of Advanced Technology during his master's degree, in 2012, and the Scholarships from the National Elites Foundation of Iran, in 2013, 2015, and 2017. He was also a recipient of the Visiting Scholarship from the Ministry of Science Research and Technology, Iran, for sabbatical leave at EPFL University, from 2017 to 2018. In 2019, he received the Ulam Programme Postdoctoral Research Grant sponsored by the Polish National Agency for Academic Exchange (NAWA). He received the High-Level Foreign Talents Postdoctoral Fellowship from China Government. He won a Competitive Grant awarded by the China Postdoctoral Science Foundation, in 2020.

JOSEP M. GUERRERO (Fellow, IEEE) received the B.S. degree in telecommunications engineering, the M.S. degree in electronics engineering, and the Ph.D. degree in power electronics from the Technical University of Catalonia, Barcelona, in 1997, 2000, and 2003, respectively. Since 2011, he has been a Full Professor with the Department of Energy Technology, Aalborg University, Denmark, where he is responsible for the Microgrid Research Program. Since 2014, he has been the Chair Professor of Shandong University. Since 2015, he has been a Distinguished Guest Professor with Hunan University. Since 2016, he has been a Visiting Professor Fellow with Aston University, U.K., and a Guest Professor with the Nanjing University of Posts and Telecommunications. In 2019, he became a Villum Investigator by the Villum Fonden, which supports the Center for Research on Microgrids (CROM) at Aalborg University, where he is the Founder and the Director. He has published more than 500 journal articles in the fields of microgrids and renewable energy systems, which are cited more than 50 000 times. His research interests include different microgrid aspects, including power electronics, distributed energy-storage systems, hierarchical and cooperative control, energy management systems, smart metering, and the Internet of Things for ac/dc microgrid clusters and islanded minigrids, with a special focus on microgrid technologies applied to offshore wind and maritime microgrids for electrical ships, vessels, ferries, and seaports. In 2015, he was promoted as a Fellow of the IEEE for his contributions on distributed power systems and microgrids. He received the Best Paper Award of the IEEE TRANSACTIONS ON ENERGY CONVERSION, for the period 2014–2015, the Best Paper Prize of IEEE-PES, in 2015, and the Best Paper Award of the IEEE OPEN JOURNAL OF POWER ELECTRONICS, in 2016. He is an Associate Editor of a number of IEEE TRANSACTIONS. From 2014 to 2019, he was awarded by the Clarivate Analytics (former Thomson Reuters) as a Highly Cited Researcher.

GIBRAN DAVID AGUNDIS TINAJERO (Member, IEEE) received the B.S. degree in mechanical and electrical engineering and the M.Sc. and Ph.D. degrees in electrical engineering from the Universidad Autónoma de San Luis Potosí, San Luis Potosí, Mexico, in 2012, 2014, and 2018, respectively. He is currently working as a Postdoctoral Fellow with the Energy Technology Department, Aalborg University, Denmark, where he contributes in different renewable-energy related projects. His research interests include modeling, analysis, and control of microgrid clusters, including LV and MV distribution grids.